Review

Microwave-Assisted Synthesis as a Promising Tool for the Preparation of Materials Containing Defective Carbon Nanostructures: Implications on Properties and Applications

Damian Pawelski and Marta E. Plonska-Brzezinska *

Posted Date: 3 August 2023

doi: 10.20944/preprints202308.0283.v1

Keywords: carbon nanostructure; defect; heteroatom doping; catalysis; electrocatalysis; electrochemistry; supercapacitor; microwave irradiation; microwave-assisted synthesis; inorganic nanoparticle

Review

Microwave-Assisted Synthesis as a Promising Tool for the Preparation of Materials Containing Defective Carbon Nanostructures: Implications on Properties and Applications

Damian Pawelski and Marta E. Plonska-Brzezinska *

Department of Organic Chemistry, Faculty of Pharmacy with the Division of Laboratory Medicine, Medical University of Bialystok, Mickiewicza 2A, 15-222 Bialystok, Poland; damian.pawelski@umb.edu.pl

* Correspondence: marta.plonska-brzezinska@umb.edu.pl

Abstract: In this review, we focus on a small section of the extensive literature that deals with the materials containing pristine defective CNs and those incorporated in the hybrid materials. We will discuss only those topics that focus on structural defects related to the introduction of perturbation into the surface topology of a nanostructure. We focus mainly on the method using microwave (MW) irradiation, which is a powerful tool for synthesizing and modifying carbon-based solid materials. In addition, the simplicity of the technique, economy, and the possibility of conducting the reaction in solvents and solid phase, in the presence of components of different chemical nature, allows use in various combinations. In this review, we will emphasize the advantages of synthesis using MW-assisted heating and indicate the influence of the structure of the obtained materials on their physical and chemical properties. We will also highlight the role of the occurrence of defects in the carbon material and the implication in designing their properties and applications.

Keywords: carbon nanostructure; defect; heteroatom doping; catalysis; electrocatalysis; electrochemistry; supercapacitor; microwave irradiation; microwave-assisted synthesis; inorganic nanoparticle

1. Introduction

The term "nanoscale" has been conventionally used to refer to size scales of 1-100 nm. Nanotechnology is now ubiquitous. It also applies to structures that are built of many atoms, forming groups called nanostructures. These consisting mainly of carbon atoms (carbon nanostructures, CNs), are among the most popular in this group. Different morphological variations of CNs, for example, nanocones [1], nanotubes [2], diamond-like carbon [3,4], onion-like carbon [5], nanofibers [1], graphene [6], and graphdiyne [7–9], have become quite well known [1,5,6,10,11]. The widespread fascination with discovering new allotropic forms of carbon materials and studying their physicochemical properties is already passing away. However, in some areas, they are still in the spotlight. For example, in materials science, CNs play a valid role in research and are considered an essential component of future materials and devices.

We are familiar with the advantages and disadvantages of CNs [12,13], which are mainly made of carbon atoms. We realize that combining several hundred or thousand carbon atoms in well-organized macromolecular systems creates interesting structures with unique properties [14]. How they are bonded defines the physicochemical properties of the formed CNs [15]. Despite almost identical chemical compositions, the CNs differ significantly in their physical properties with different dimensionality and chemical reactivity [14]. These greatly affect their subsequent use in many areas, mainly in electronics [16,17], catalysis [18,19], energy conversion and storage [20], sensors [21–23], for biomedical [24], for biological and environmental applications [25–27].

The electrochemical properties of carbon-based electrode materials are closely related to their chemical composition, structure and defects [28–30]. Among all the candidates, graphene-like and graphitic materials are perceived to be ideal for catalysis, electrocatalysis and electrochemistry due

to their excellent conductivity and mechanical stability, large specific area with microporosity, easy production of defective motifs in their structures (e.g., pentagon defects, edge defects, hole defects from micropores) and high charged carrier mobility [31–34].

In this review, we focus on the materials containing pristine defective CNs (d-CNs) and those incorporated in the hybrid materials. We focus mainly on the method using microwave (MW) irradiation for the synthesis and modification of materials. A simplicity of the method, economy, the possibility of conducting the reaction in solvents and solid phase, in the presence of components of different chemical nature, allows to use it in various combinations. We will emphasize the advantages of synthesis using MW-assisted heating, their chemical and physical properties and applications.

2. Definition of defective CNs

Defects are widely present in nanomaterials, and they are recognized as the 'active sites' for reactions, which tune electronic and surface properties in the local region [35–37]. Concerning the dimensions, defects in solid nanomaterials can be classified into four categories [35,38–40]:

(a) zero-dimensional (0D) point defects (e.g., doping, vacancy, reconstruction), which can be further divided to:
   - reconstructed or vacancy defects,
   - non-metallic-atom-doping induced defects,
   - metal defects [36,41];
(b) one-dimensional (1D) line defects (e.g., dislocation);
(c) two-dimensional (2D) planar defects (e.g., grain boundary)
(d) three-dimensional (3D) volume defects (e.g., spatial lattice disorder).

The disorder in the crystal structure is related to the ideal lattice structure [42,43]. **Point defects** are defects on a tiny scale, referring even to the defect of a single atom in the crystal. Due to the location of this defect, we distinguish among them vacancy, interstitial defect, replacement, and antisite. **Line defects** are related to disturbances in the crystal structure along the crystalline (for example, dislocation, steps). **Surface defects** have a very diverse nature. It is defined as any disturbance of the crystal structure in one direction. Here we can indicate, for example, twin crystals, grain boundary, etc. And the last group of defects, the largest in their scale, is defects of the structure in three dimensions.

A division of defects is also introduced, considering materials' physical and chemical properties. Here we can distinguish thermal defects (Frenkel and Schottky defects), heteroatom-doping (doping defects), electron defects in crystal, and nonstoichiometric structured defects. No matter how the structural defects in CNs are subdivided, they refer to some disturbance of the structure compared to the 'ideal structure' of this nanomaterial. This 'disturbance' leads to a change in some specific features of the nascent nanostructure, consequently modifying the physical and chemical properties of the CNs.

3. Physical and chemical properties of defective CNs with relevance in catalysis, electrocatalysis and electrochemistry

Carbon itself acts as a catalyst or material with satisfactory electrochemical performance. However, amorphous or disordered carbon materials exhibit low activity, chemical, thermal and electrochemical stability, and oxidation resistance [44–46]. The combination of carbon atoms in a 2D or 3D manner increases its stability, and at the same time, an organized macromolecular architecture defines its physical and chemical properties. As for photocatalysis [47,48], electrocatalysis [49,50] and electrochemical capacitors [29,51,52], reactions usually occur on the contact interface between catalytic or electronic materials and reactive species. Thus, the reactive interface and its physical and chemical properties are crucial for an effective reaction. *Defects modify the electronic structure of CNs and optimize the chemisorption of the key intermediates, which should trigger enhanced kinetics for improved electrocatalytic performance* [53].

Microstructural variations of CNTs are strongly connected with their conductivity and field emission. High-performance field emission (FE) requires low turn-on and threshold fields, good

Preprints (www.preprints.org) | NOT PEER-REVIEWED | Posted: 3 August 2023 doi:10.20944/preprints202308.0283.v1

electrical and mechanical stability, and dense and uniform emission sites [54]. The CNTs with excellent conductivity meet the criteria shown above. In Figure 1b,d, on TEM images, the influence of the MW-assisted hydrogen plasma process on the structural changes of the CNs was presented. The thinned and open-ended caps of the CNTs can yield larger FE. A schematic representation of the FE process is illustrated in Figure 1g. The analysis of the intensity ratio of D- and G-peaks (I_D/I_G) enabled to qualitative evaluate the formation of the CNT's defects after the plasma processing. Increasing the intensity of I_D/I_G with increasing irradiation time indicates the formation of defects in the structure of CNTs. The created sp^3-hybridized defects (defected graphite) on the CNT's walls may act as new emission sites [55,56]. Figure 1f shows FE *J*-E curves of the CNTs and CNTs modified at MW irradiation (200 W, 30 and 60 min.) in terms of emission current density. Analysis of the curves indicates typical *F-N-type* behavior [57]. The determined work function for the hydrogen plasma process (4.75 eV) is attributed to the increased state density of defects after plasma processing. FE stability of the CNTs and CNTs modified at MW irradiation (400 W, 60 min.) is presented in terms of *J* vs. time. As is shown in Figure 1e, hydrogen plasma processing affects the stability of the obtained material. Summarizing, both phenomena affect increasing electron transferring traces and enhance CNT's FE performance.

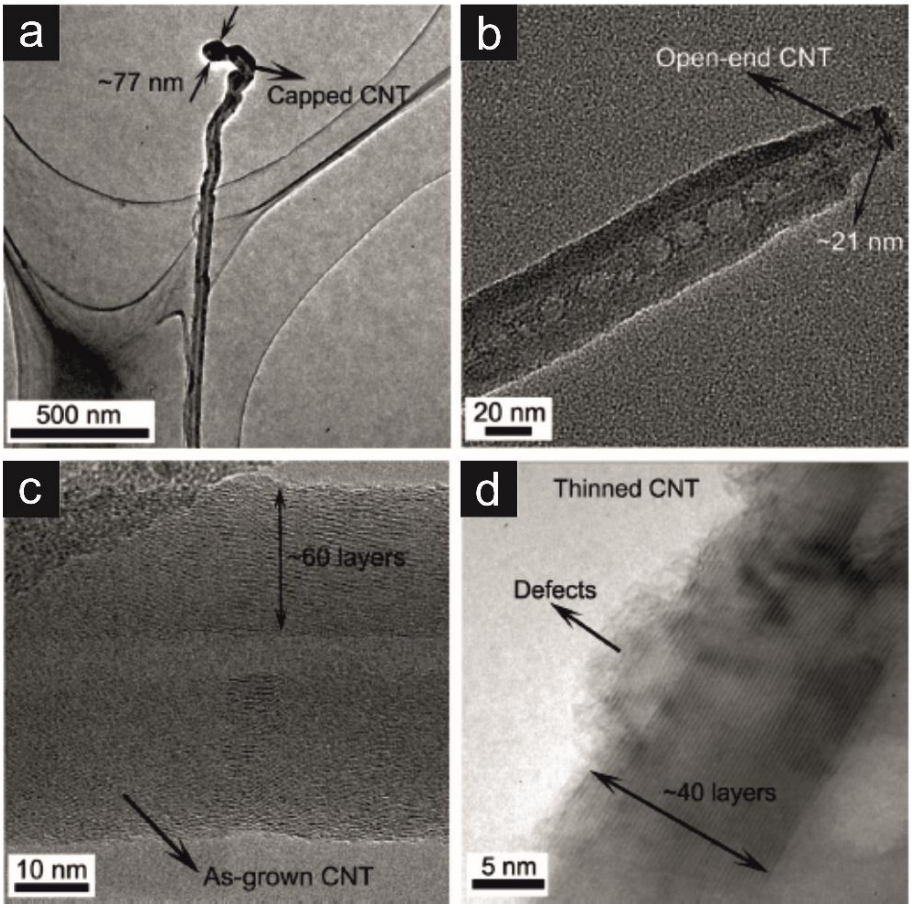

Figure 1. Low resolution TEM images of (a) a capped CNTs and (b) a thinned and open-ended CNTs. HR-TEM images of (c) an as-grown CNTS with 60 layers and (d) an MW-assisted hydrogen plasma processed CNT with ~40 layers and defected outer shells. Reprinted with the permission from Elsevier, Ref. [54].

Another important parameter known to influence electrocatalytic and electrochemical properties is surface chemistry [58–61]. The chemical functionalization of the surface through heteroatom incorporation, defect engineering, and structure modulation can provide efficient approach to enhance the catalytic activity. When the non-metal dopants are introduced into the carbon layer, they may lead to charge polarization between the heteroatom-doped and the adjacent

Preprints (www.preprints.org) | NOT PEER-REVIEWED | Posted: 3 August 2023 doi:10.20944/preprints202308.0283.v1

C atoms due to their different electronegativity [53]. When the non-metal dopants are introduced into the carbon layer, they may lead to charge polarization between the heteroatom-doped and the adjacent C atoms due to their different electronegativity [53,62]. The six non-metallic heteroatoms with various electron negativities were selected (Figure 2) [62], which act as active sites for catalytic and electrocatalytic processes:

(i). N and O acting as electron acceptors for the adjacent C [41,63–65],
(ii). B, F, S and P acting as electron donors for the adjacent C [66–68].

Some examples of heteroatom doping are presented in Table 1. The heteroatom incorporation could trigger electron transfer to enhance the electrical conductivity of CNs. On the other hand, the electrical conductivity is determined by the carrier concentration, specific band structure near the Fermi level, and charge distribution [61]. These carbon defect-based motifs tailor the local charge in graphene layers and lead to the improvement of the catalytic effect, which is mainly influenced by the nature and amount of the doped heteroatoms [41,69–71]. The latter results from the doping process using various substrates and methods. We can distinguish thermal annealing at the gaseous atmosphere and pressure [63,72,73], pyrolysis [63], chemical vapor deposition [74], MW-assisted synthesis [75], arc-discharge evaporation [76], etc. Some of these methods are used as one-step processes; others must be supported by multi-step strategies that optimize the reaction conditions.

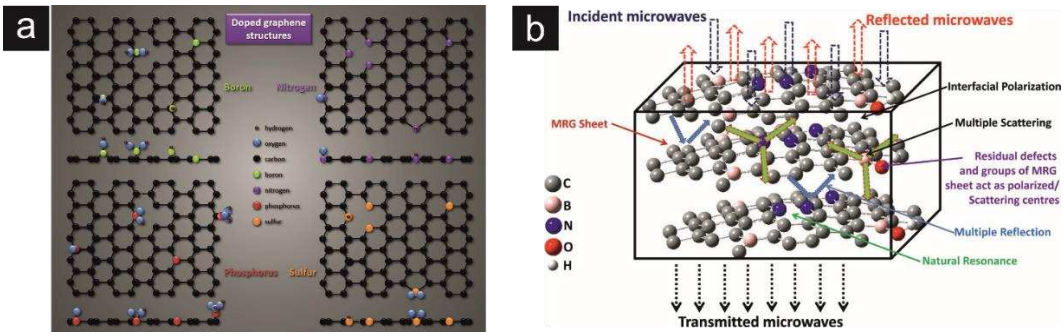

Figure 2. (a) Schematic representation of possible positions for dopant atoms in the graphene network. In each case, the normal and cross-sectional views of the doped material are provided for easier visualization. The representation does not include the actual number of chemical bonds between the elements. Reprinted with the permission from Elsevier, Ref. [62], (b) Schematic representation of possible MW absorption mechanism in B–N–MRG Sample. Reprinted with the permission from American Chemical Society, Ref. [77].

Table 1. Some examples of CNs doped by heteroatoms and their short characteristic.

Heteroatom doping	Substrates	Carbon nanostructures	Methods	Applications	Ref.
Nitrogen	Collagen	OLC	Thermal annealing	ORR catalysis	[72]
	Acetonitrile	CNO	Pyrolysis	ORR catalysis Nitride sensor	[78]
	Graphene Acetonitrile	Graphene	CVD	Supercapacitor	[74]
	Graphene Melamine	Graphene	Thermal annealing	ORR, OER, HER catalysis	[79]
	Melamine L-cysteine	Graphene	Polymerization Pyrolysis	ORR and OER catalysis Zn-air batteries	[41]
	CNT Ionic liquid	CNT/porous carbon (Core-sheath)	Carbonization Post-modification	ORR catalysis	[73]

Preprints (www.preprints.org) | NOT PEER-REVIEWED | Posted: 3 August 2023 doi:10.20944/preprints202308.0283.v1

	CNT Melamine	CNT/porous carbon	Pyrolysis Polymerization Post-modification	ORR catalysis Zn-air batteries	[80]
	Citric acid Urea Aniline	GQD	MW-assisted hydrothermal process Polymerization	Gas sensing	[81]
	Acetonitrile, pyridine, amine N_2 gas atmosphere	Carbon nanoflakes	Hard-templating Pyrolysis	Electrochemistry	[82]
Halogen (F, Cl, Br, I)	Graphite Halogen-containing acids	rGO	Electrochemical exfoliation/post-modification GO	ORR catalysis	[83]
Sulfur	Melamine Thiourea	Graphitic carbon nitride (g-C_3N_4) nanoflakes	Pyrolysis	NO_2 gas sensors	[63]
Multi-heteroatoms	Compounds containing S, O, N, C	CNT (S, O, N)	Post-modification	ORR catalysis	[84]
	Compounds containing O, N, C	CNT (N, O)	Post-modification	ORR catalysis	[64]
	Solid graphite rod Nitrogen atmosphere Amorphous boron	CNT (N, B)	Arc-discharge evaporation	Conductors Magnetoconductors	[76]
	Melamine Phosphoric acid	Graphitic carbon nitride (P)	Thermal annealing	ORR catalysis	[85]
	Citric acid L-cysteine	GQD (N, S)	Hard-templating Carbonization	Fluorescence detection of Fe^{3+}	[86]
	ND Boric acid	CNO (N, B)	Thermal annealing	ORR catalysis	[87]
	Olive oil Nitric acid	CNO (N, O)	Pyrolysis CVD	Fuel cells	[75]
	Benzene	Carbon nanocages (O, N)	Hard-templating Thermal annealing	ORR catalysis	[31]

* Abbreviations in alphabetical order. CNO: carbon nano-onion; CNT: carbon nanotube; CVD: chemical vapour deposition; GO: graphene oxide; GQD: graphene quantum dot; HER: hydrogen evolution reaction; ND: nanodiamond; OER: oxygen evolution reaction; OLC: onion-like carbon; ORR: oxygen reduction reaction; rGO: reduced graphene oxide.

Doping is a critical process that significantly affects the conductive properties of carbon materials, creating electron holes (p-type doping) in the graphene layer or places with an excess negative charge (n-type doping) [88]. The authors observed the synergistic effect of two kinds of heteroatom-doping (B- and N-co-doped and P- and N-co-doped CNs), where the electron transfer and reaction energy in ORR and oxygen evolution reaction (OER) was strongly affected by co-doping [66,68,89]. It should be noted that only some atomic configurations are preferred. Density functional theory calculations indicated that the chemical coupling of B- and N-pyridinic active sites boosts the ORR activity when the distance between two atoms is small [89,90].

Because the π-conjugation, sp^2-hybridized CNs can serve as electron donors or acceptors when coupled with other elements with different electronegativity. The carbon π electrons are triggered by breaking the integrity of π-conjugation [31]. N-doped CNs are activated by conjugating with the lone-pair electrons from N dopants, and as a result, the C atoms neighboring N become ORR active [31].

Preprints (www.preprints.org) | NOT PEER-REVIEWED | Posted: 3 August 2023 doi:10.20944/preprints202308.0283.v1

There is a hot debate on which type of N atoms (graphitic N or pyridinic N) is favorable in ORR activity [91]. *The most recent theoretical research demonstrates that the C atoms with Lewis basicity adjacent to pyridinic N are the active sites for the ORR* [67]. The carbon π electrons in B-doped CNs are activated by conjugating with the vacant $2p_z$ orbital of B. In these nanostructures, the B sites become active for ORR [31]. In acidic electrolytes, CNs co-doped with N and S are very promising [30]. The presence of N-C-S-defect-based motifs in carbon materials decreased the energy barriers for ORR in acidic solutions. The half-wave potential was lower than that of Pt/C commercial electrocatalyst [30].

Apart from doping elements, *other factors such as surface area/porosity/morphology of the materials affect the catalytic activities* [53]. CNs easily form pores of different sizes (micro-, meso- and macropores) owing to their flexible bonding and surface properties. The porous structures and the different pore size may affect different steps involved in the catalytic reaction:

(i). micro-pores allow more active sites into the electrolyte,
(ii). meso-pores can facilitate the mass transport in the catalyst layer,
(iii). macro-pores ensure the long-term stability of the catalyst [53].

Zheng Hu and coworkers presented an exciting example of carbon nanocages preparation and the influence of defective CNs on electrocatalytic activity in 2015 [31]. Carbon nanocages were synthesized by the hard-templating method from benzene as the precursor. The pyrolysis at the different temperatures (700, 800 and 900°C) results in the formation of carbon nanocages with a cuboidal hollow structure 10–20 nm in size with a shell thickness of four to seven graphitic layers (Figure 3a). Increasing the temperature led to increasing of the average size and wall thickness of the nanocages, and simultaneously, to decreasing specific surface areas of 1713 m^2/g (700°C), 1009 m^2/g (800°C), and 614 m^2/g (900°C). Temperature also affects the distribution of pores and the number of defects in the structure. Micropores (~0.6 nm) and mesopores (5–50 nm) coexist in the materials. However, an increase in temperature causes the pore distribution to shift towards the mesopores (Figure 3b). As the temperature increases, the crystallinity of the material increases, i.e., the number of defects in the material decreases (Figure 3c). The highest concentrations of the defects was detected for the material pyrolyzed at 700°C. Defects in carbon nanocages are recognized as the topological disclinations at the corner, the surficial broken fringes, and the holes through the shell (Figure 3d). *The theoretical and experimental studies showed that zigzag edge and pentagon defects are responsible for the electrocatalytic activity of carbon nanocages.*

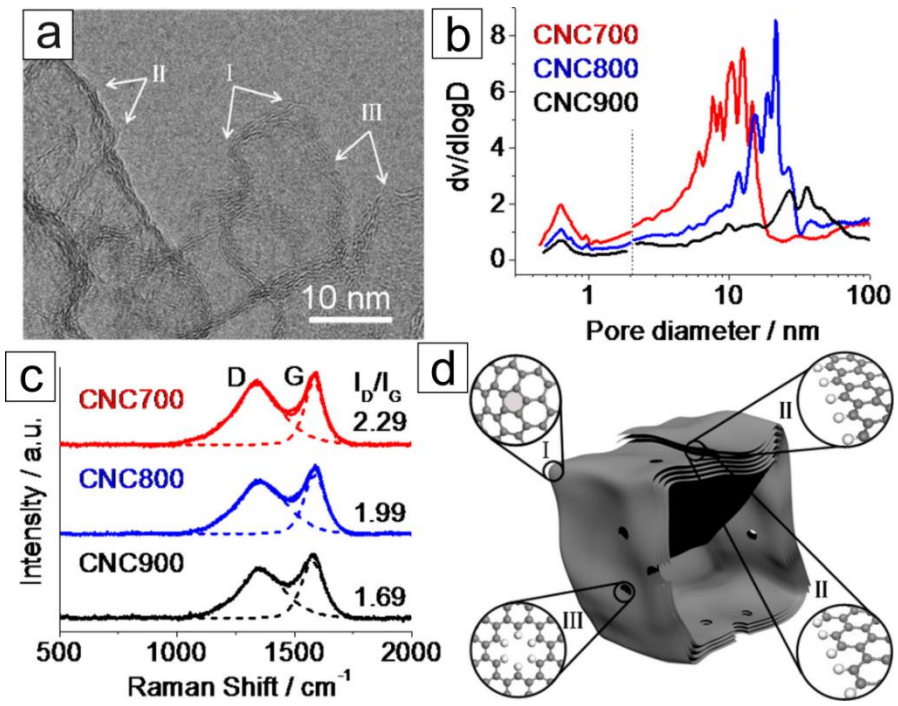

Figure 3. Characterizations and schematic structural characters of the carbon nanocages. (a) HR-TEM image of CNC700. (b) Pore size distributions. (c) Raman spectra. I_D/I_G is the area ratio of the D peak

 doi:10.20944/preprints202308.0283.v1

to the G peak. (d) Schematic structural characters of the carbon nanocages. I, II, and III in panels a and d represent three typical defective locations, i.e., the corner, the broken fringe, and the hole, respectively. Reprinted with the permission from American Chemical Society, Ref. [31].

Carbon materials used as active materials in capacitors show direct relationship between the electrostatic capacitance and their specific surface area (SSA) values [92]. However, the increase of the specific capacitance is only observed for low SSA values, but it tends to plateau rapidly. Therefore, how the surface is developed significantly impacts the value of specific capacitance achieved [92]. For example, carbon nanoonions (CNOs) derived from NDs in the temperature range between 1,300 and 1,800°C have displayed high SSA values. The SSA values determined by N_2 gas adsorption were between 380 and 680 m^2/g [93], which is lower than that of many carbon materials. Still, it is *fully accessible for ion adsorption* due to the absence of a porous network inside the particles [94,95].

Nanoscale systems do not directly comply with the above rules. In this case, the nanoscale and quantum effects must be frequently considered. The nanoscale implies a large surface area to volume ratio, indicating the enhanced role of the surface for capacitive storage [96]. Indeed, more than the total porous volume, the pores' formation (pore size and distribution) is more important. *In addition, the carbon defects such as dislocation, atom vacancies and stacking faults constitute the active sites area (active surface area, ASA)* [97]. It is an intrinsic structural characteristic of graphitic CNs [98]. Several experimental, as well as theoretical studies, have shown that the experimental conditions during temperature annealing treatments have an influence on ASA of the CNs [98]. The studies confirmed that defects in graphitized carbons at the nanoscale play a significant role in enhancing the electrochemical behavior in aqueous electrolytes. A comparison between different energy storage devices designed for microelectronics power applications showed that using the 'small' spherical nanostructures resulted in high power and high energy [99]. Compared to conventional carbon black and graphite nanoparticles, for example CNOs consistently lead to better gravimetric and volumetric performance [12,99].

4. MW-assisted synthesis for the preparation and modification of materials containing defective CNs

4.1. Definition of MW-assisted synthesis

Microwave-assisted (MW) irradiation is a powerful heating method for carbon-based solid materials because they are usually very good absorbents of MW irradiation [100,101]. This high-frequency electromagnetic radiation with a wavelength between 0.001 and 1 m (frequencies between 300 and 0.3 GHz) can achieve a temperature of over 1,000°C within a few minutes. Heating of the material is possible due to the interaction of charged particles in some materials with the electric field, which is a component of electromagnetic radiation of appropriate energy [102,103]. When polar molecules interact with MW radiation, this causes them to rotate and move, and this, in turn, causes friction. Consequently, the generated energy is dissipated as heat (*dipolar polarization*). In the case of solid phase materials that are dielectrics, charged particles such as pi electrons in carbon materials induce a current flow in the material. In this case, the energy is also dissipated as heat, which is related to the Maxwell-Wagner effect (*interfacial polarization*). For the optimal interaction of MW with solid materials, its penetration depth also has to be considered when using the MW heating method [102]. However, it has to be noted that penetration depth becomes a critical factor in micron-scale materials. For the materials in the nanoscale, this problem should not occur.

Major advantages of using MW heating [101]:

- ✓ contactless heating;
- ✓ a direct transfer of energy to the reactants;
- ✓ independence from heat convection;
- ✓ rapid heating rates;
- ✓ easy control of irradiation parameters;
- ✓ selectivity of heating, the possibility of conducting the reaction locally and volumetrically.

The MW-based methods may be divided into two groups:

Preprints (www.preprints.org) | NOT PEER-REVIEWED | Posted: 3 August 2023 doi:10.20944/preprints202308.0283.v1

- ✓ ***top-down***; methods, which include the transformation of solid materials into carbon nanomaterials;
- ✓ ***bottom-up***; methods, which include the preparation of carbon nanomaterials from liquid or gaseous carbonaceous precursors.

It is possible to use the energy of the MW irradiation to create new carbon materials and as a method for purification, functionalization or annealing of CNs [103]. It is often a method supporting other processes and procedures. Depending on the specific structural properties of the CNs, MW irradiation interacts specifically with the material due to the particular absorption properties of the CNs [104]. The temperature reached in a given process will depend on many parameters. Depending on the type of CNs, their purity (for example, metallic dopants), the defects structure, functional groups on the surface (for example, containing oxygen), and during the interaction of the carbon material with MW irradiation, local heating may occur. Conversely, when the carbonaceous material is a poor absorber of MW irradiation, it is necessary to add substances to make the MW heating process more efficient [102,105]. In this case, substances such as polymers, conducting materials or ionic materials, metallic nanoparticles, etc., are added [106–108].

4.2. MW-assisted synthesis for the preparation and modification of defective CNs: implications on properties and applications

MW-assisted synthesis is a powerful heating method for preparing or modifying carbon-based solid materials [109]. Currently, this method is most often used to design and modify graphene (G), carbon nanotubes (CNTs), carbon quantum dots (CQDs) and nitride carbon. By MW-assisted heating with the different carbon source (graphite [110,111], metallocenes [104,111], carbon nanoparticles [112], polymers [113,114], etc.), the power and reaction time, in the presence of catalyst and in the gas phase, different CNs were synthesized. Some examples with a brief description are presented in Table 2.

Table 2. Some examples of using MW-assisted synthesis for the preparation and modification of pristine d-CNs and hybrid materials containing d-CNs.

Defective CNs	Materials containing d-CNs	Methods Parameters	Applications	Refs.
Pristine d-CNs	d-G (hydrogel)	MW-assisted synthesis (800 W; 5 min.) Hydrothermal process	Supercapacitors (340 F/g at 0.5 A/g)	[115]
	N,S-GO	MW-assisted synthesis (800 W; 5 min.)	Supercapacitors	[88]
	S-rGO	MW-assisted synthesis (140°C; 30 min.)	Supercapacitors (238 F/g)	[116]
	N,B-rGO	MW-assisted synthesis	EMI shielding devices	[77]
	rGO (porous)	MW-assisted synthesis (700 W; 180°C; 6 min.)	Supercapacitors (568 F/g at 1 A/g)	[117]
	rGO	IL-assisted MW synthesis (700 W; 15 s.)	Supercapacitors (135 F/g; 58 Wh/kg; 246 kW/kg)	[118]

Preprints (www.preprints.org) | NOT PEER-REVIEWED | Posted: 3 August 2023 doi:10.20944/preprints202308.0283.v1

Hybrid materials containing d-CNs	d-CNT	MW hydrogen plasma processing	Vacuum electron sources	[54]
	d-CNT	MW-assisted synthesis (C_2H_2/H_2, 0.6 ratio; 900 W; 35 min.)	Sorbents (removing organic pollutants from wastewater)	[119]
	N-CQD/ox-MWCNT	MW-assisted synthesis (700 W; 10 min.)	Electrocatalysis DSSC	[120]
	GO/g-C_3N_4	Ultrasonic-MW-assisted synthesis (700 W; 5 min.)	Photocatalytic H_2 evolution	[121]
	N-PGF	MW-assisted synthesis (800 W; 4 s.)	Supercapacitors (12.3 mW h/cm; 0.42 W/cm) Sorbents	[122]
	CNT/Fe_2O_3	CVD growth of CNTs Hard templating Hydrothermal method MW-assisted synthesis	Lithium-Ion Battery Electrodes	[123]
	N-MWCNT/Fe_3O_4	CVD growth of MWCNTs MW-assisted solvothermal synthesis (800 W; 1.5 min.)	Superparamagnetic materials	[124]
	CNT/$NiMn_2O_4$	MW-assisted hydrothermal synthesis (800 W; 160°C; 1 h)	Supercapacitors (916 F/g at 1 A/g; 36.5 Wh/kg; 800 W/kg)	[125]
	MWCNT/$CoMoO_4$	MW-assisted solid-state synthesis (480 W; 8 min.; 720 W; 7 min.)	Supercapacitors (170 F/g at 0.1 A/g)	[126]
	NiS@CNT/NiO	MW-assisted solid-state synthesis (1000 W; 60 s.)	Supercapacitors (810 F/g at 1 A/g)	[127]
	ox-CNT/*o*-PDA-*co*-ANI	MW-assisted synthesis	Supercapacitors (147 F/g at 0.5 A/g)	[128]
	rGO/NiS	MW-assisted hydrothermal synthesis (700 W; 4 min.)	Supercapacitors (1746 F/g at 1 A/g) Solid-state Supercapacitors (14.20 F/g; 7.1 Wh/kg; 1836 W/kg)	[129]
	rGO/Fe_3O_4	Chemical exfoliation MW-assisted synthesis	Lithium-Ion Battery Electrodes	[130]

Preprints (www.preprints.org) | NOT PEER-REVIEWED | Posted: 3 August 2023 doi:10.20944/preprints202308.0283.v1

	(700 W; 1.25-1.75 min.)		
rGO/CNT/Ni_{NP}	Thermal exfoliation MW-assisted synthesis (700 W; 5 min.)	Lithium-Ion Battery Electrodes	[131]
GO/NiO	Exfoliation MW-assisted synthesis	Energy storage devices (549 F/g at 10 mV/s)	[132]
rGO/NiO/Co_3O_4	MW-assisted synthesis (700 W; 45 sec.)	Supercapacitors	[133]
rGO/CoAl-LDH	MW-assisted reflux synthesis (1000 W; 100°C; 2 h)	Supercapacitors	[134]
rGO/NiAl-LDH	MW-assisted reflux synthesis (1000 W; 100°C; 2 h)	Supercapacitors	[135]
rGO/$NiMoO_4$	MW-solvothermal synthesis (200 W; 115°C; 25 min.) Thermal annealing	Supercapacitors	[136]
N-G/NiS	MW-assisted synthesis	Supercapacitors (1468 F/g at 1 A/g; 66.6 Wh/kg; 405.8 W/kg)	[137]
rGO/$MnCo_2O_4$	Exfoliation Reduction MW-assisted synthesis (900 W; 45, 55 and 70 s)	Supercapacitors (562 F/g at 20 mV/s)	[138]
G/α-MoO_3	MW-assisted synthesis (700 W; 7 min.)	Supercapacitors (483 F/g at 1 A/g)	[139]
rGO/$CoSe_2$	MW-assisted synthesis (700 W; 7 min.) Thermal annealing	Supercapacitors (761 F/g at 1 A/g; 43.1 Wh/kg) LED	[140]
G/Co_9S_8	MW-assisted hydrothermal synthesis (700 W; 160°C; 30 min.; $8 \cdot 10^6$ Pa)	Supercapacitors (1150 F/g at 5 mV/s)	[141]
rGO/MnN	MW-assisted synthesis (900 W; 1 min.)	Sodium ion batteries Supercapacitors EMI shielding	[142]
rGO/MnO_2	Conventional synthesis	Supercapacitors (140 F/g at 1 A/g)	[143]

Preprints (www.preprints.org) | NOT PEER-REVIEWED | Posted: 3 August 2023 doi:10.20944/preprints202308.0283.v1

	MW-assisted synthesis (700 W; 2 min.; 21 cycles)		
N-rGO/Pd	MW-assisted synthesis (900 W; 1 min.)	Direct-Ethanol Fuel Cells	[144]
rGO/Pd	MW-assisted synthesis	Electrocatalysis (Ethanol Oxidation)	[145]
S-rGO/$NiFeS_2$	MW-assisted synthesis	Supercapacitors (1073 F/g at 1 A/g; 45.7 Wh/kg; 222 W/kg)	[146]
3D Pd-E-PG	MW-assisted synthesis (700÷900 W; 30÷60 sec.)	H_2 storage CO oxidation	[147]
NiF-G/SimonK	MW-hydrothermal synthesis	Supercapacitors (836 F/g at 1 A/g)	[148]
G/NiCoS	MW-assisted synthesis (600 W; 20 min.)	Supercapacitors (1186 F/g at 1 A/g; 46.4 Wh/kg)	[149]
G/CNT/Pd	IL-assisted MW synthesis	Energy storage systems (1615 F/g at 10 mV/s)	[150]
CMK-3/CNT	Hard-templating method MW-assisted synthesis (700 W; 30 s.)	Supercapacitors (315 F/g at 1 A/g)	[151]

* Abbreviations in alphabetical order. CMK-3: ordered mesoporous carbon; CNT: carbon nanotubes; CQD: carbon quantum dot; d-CNT: defective carbon nanotube; DSSC: dye-sensitized solar cells; EMI: electromagnetic interference; G: graphene; GO: graphene oxide; rGO: reduced graphene oxide; g-C_3N_4: graphitic carbon nitride; LDH: layered double hydroxide; LED: light emitting diode; MnN: manganese nitride; MWCNT: multi-walled carbon nanotube; N-PGF: nitrogen-doped porous graphene framework: NCS: nickel cobalt sulfides; NiF: nickel foam; ox-CNT: oxidized carbon nanotubes; *o*-PDA-*co*-PANI: copolymer of *ortho*-phenylenediamine and aniline; 3D Pd-E-PG: Pd-embedded three dimensional porous graphene; SimonK: Simonkolleite ($Zn_5(OH)_8Cl_2 \cdot H_2O$).

Figure 4 presents two examples of MW irradiation's use for synthesizing different compositions of carbon-based materials. Panel (I) shows the preparation of N-CQD/MWCNT material using the conventional method and MW-assisted synthesis [120]. The first stage of the process was based on the most popular way of MWCNT oxidation using concentrated nitric acid. As a result of this reaction, oxygen-containing functional groups were introduced on the MWCNT surface. In the further stage of the reaction, these sites, called structural defects, are active sites for further functionalization.

Further, in the presence of urea and citric acids and under heating, nitrogen-doped carbon quantum dots are formed on the surface of MWCNTs (Panel (I), Figure 4). The authors of this work also carried out, for comparison, the stage of N-CQD production under conventional reaction conditions. The data summarized in the table indicate that using MW irradiation to synthesize N-CQDs shortens the reaction time and energy consumption and increases the efficiency of the reaction.

Panel (II), Figure 4 shows the possibility of multifunctional use of MW irradiation, depending on the power and duration of its use. Kumar and colleagues used the MW irradiation process to obtain nanohole-structured and Pd-embedded 3D porous graphene (3D Pd-E-PG) [147]. The process

Preprints (www.preprints.org) | NOT PEER-REVIEWED | Posted: 3 August 2023 doi:10.20944/preprints202308.0283.v1

was multi-stage, but thanks to the short times of using MW irradiation, it was easy to perform, as shown schematically in the figure. The first stage was graphene's exfoliation and adding ethanol and palladium acetate to the reaction mixture.

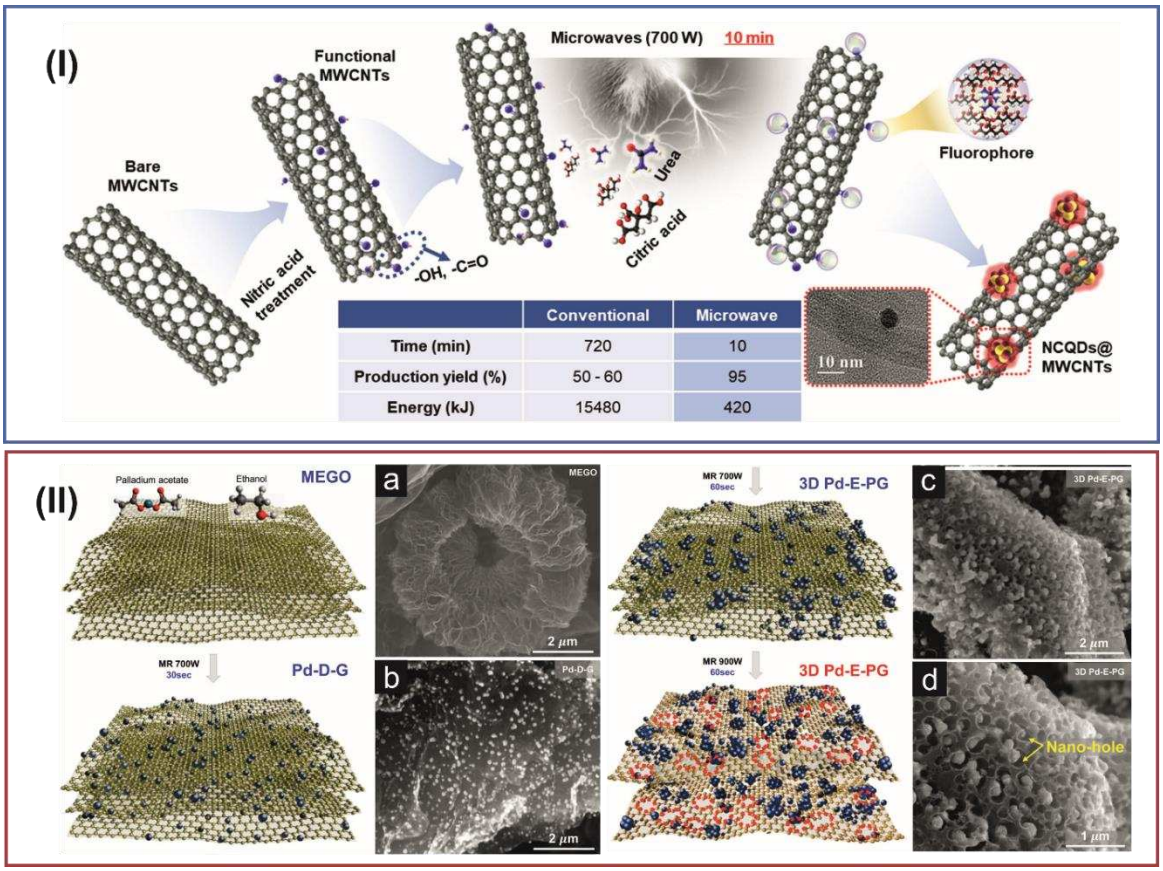

Figure 4. Panel (I): Schematic illustration of synthesis of MWCNT/NCQD, where mild oxidation generates active sites for the growth of NCQDs. The inset table compares the conventional synthesis with MW-assisted process. Reprinted with the permission from Elsevier, Ref. [120]. **Panel (II):** Synthesis route of nanohole-structured and Pd-embedded 3D porous graphene (3D Pd-E-PG) and corresponding SEM images. Schematic illustration of the MW fabrication process of the 3D Pd-E-PG. (a) SEM image of MW-exfoliated graphene oxide. (b) SEM image of the uniform decoration of Pd nanoparticles on graphene layers after low-power MW irradiation. (c) SEM image of the aggregation of Pd nanoparticles after successive high-power MW irradiation. (d) SEM image of nanohole generation and the perforated graphene structures after multistep MW irradiation. Reprinted with the permission from American Chemical Society. Ref. [147].

Then, under the influence of MW irradiation with a power of 700 W, within 30 sec. Pd nanoparticles were created. Next, MW irradiation with a power of 700 W for 60 s was applied again, which caused the formation of a 3D structure consisting mainly of agglomeration of Pd nanoparticles. In the last stage of the process, a higher power MW irradiation (900 W, 60 s) was used, which caused the perforation of graphene layer (creation of defects). Holes of a size analogous to Pd nanoparticles enabled the distribution of nanoparticles in the entire volume of the carbon material, creating a compact and interconnected structure of 3D Pd-E-PG. The course of each stage was confirmed by scanning electron microscopy (SEM) imaging (Figure 4a-d, Panel (II)). Figure 4a (II) shows the graphene layers, which, as a result of MW irradiation form a brush-like and wrinkled structure. In the next stage, the Pd nanoparticles are evenly distributed on the graphene layers (Figure 4b (II)). As a result of MW irradiation of a certain time and power, the graphene layers are covered with a large amount of Pd nanoparticles. Further irradiation leads to the formation of nanoholes (10-100 nm)

 doi:10.20944/preprints202308.0283.v1

(Figure 4c (II) and Figure 4d (II)), in which metallic nanoparticles are placed, creating a 3D structure of Pd-E-PG, with the simultaneous formation of increasingly larger metallic agglomerates.

Generally, the synthesis or modification of carbon-based materials using MW irradiation follows the presented paths. In some cases, it is necessary to run the reaction in multiple steps, mainly to increase the yield of the reaction. Despite this, the procedures are much more straightforward, thanks to the short reaction times under MW-assisted heating. In addition, in the case of these methods, the purification process is much simpler.

Graphene is a 2D atomic crystal with extreme mechanical strength and high electronic and thermal conductivities. Due to these outstanding properties, it has been one of the most frequently used CNs in scientific research in recent years. In the case of this carbon structure, MW irradiation is not used to prepare it in bottom-up processes. However, MW irradiation is used to modify graphite precursors due to its simplicity. Exfoliation is therefore possible, yielding graphene oxide (GO) [152]; reduction of GO [115], resulting in reduced GO (rGO) [117]; doping of graphene layers with heteroatoms [88,116,118] or combination of two kinds CNs in one material [121,122].

MW irradiation is often used to functionalize graphene layers. Controlled creation of defects in graphene based materials is a promising strategy to tailor the electrical, electrochemical, and electrocatalytic properties. For example, a hydrogel was obtained from oxidized graphene during MW-assisted synthesis in hydrothermal conditions (Figure 5a) [115]. This one-step process resulted in a 3D carbon structure resembling crinkled paper. Such a 3D graphene structure can accelerate the transport and diffusion of ions, and functional groups reduce the aggregation of graphene layers. The obtained material exhibits a high specific capacitance (*Cs*) of 340 F/g at the current density of 0.5 A/g and excellent stability with approximately 97.3% retention of the initial *Cs* after 20,000 cycles (at 10 A/g) (Table 2). These parameters indicate that d-G (hydrogel) may be a promising electrode material for high-performance supercapacitors.

Analogous conditions were also used to obtain GO-based gelatin aerogels (Figs. 5B and 5e) [152]. In binary aerogel, non-covalent and covalent interactions are under acidic and alkaline conditions. The modulus of elasticity increased 6-fold and 1.38-fold, and the swelling ratio (SR) increased 1.2-fold and 1.4-fold for aerogels at acidic and alkaline pH, respectively, when the gelatin content increased. In addition, a higher SR value was found for the aerogel synthesized in an alkaline environment. The properties of the aerogel obtained using MW irradiation were compared with this synthesized using conventional heating. Similar physicochemical properties of both aerogels were identified; however, the SR value was 1.5 times higher for the aerogel synthesized using MW irradiation.

The following example shows the possibility of using the MW-assisted method to produce porous reduced graphene oxide (rGO) (Figs. 5e and 5f) [117]. Conducting the synthesis under MW irradiation conditions causes a shorter period and lower temperature employing hydrochloric acid as an etching agent. In addition to lowering energy consumption, preparing the material under these conditions leads to obtaining material that avoids the restacking of subsequent rGO layers and numerous pores and promotes the improvement of material transport efficiency. It is a critical phenomenon because reduced GO is characterized by a strong stacking effect of individual graphene layers, which significantly limits the potential of using this material in devices that accumulate electric charge. The combined macro/mesopore effect in porous rGO provides accessible ion transport pathways for the base electrolyte compared to conventionally prepared rGO. The electrochemical studies show, that for the synthesized rGO calculated *Cs* was 568.5 F/g at 1 A/g with a remarkable capacity retention after longer charge/discharge cycles (Table 2).

An exciting example of using MW irradiation to modify GO is the method presented by Kwang S. Suh et al. [118]. The proposed facile and scalable method leads to the production of rGO by ionic liquid-assisted MW chemistry. Ionic liquids were used as sources of dipoles and the doping element rGO. The resulting material is characterized by the open porous architecture of rGO filled with IL moieties that results of easy ions transportation, and consequently exhibited a high *Cs* of 135 F/g. Additionally, a device operated at a voltage of 3.5 V exhibited a high energy density (~58 Wh/kg) and power density (246 kW/kg).

Preprints (www.preprints.org) | NOT PEER-REVIEWED | Posted: 3 August 2023 doi:10.20944/preprints202308.0283.v1

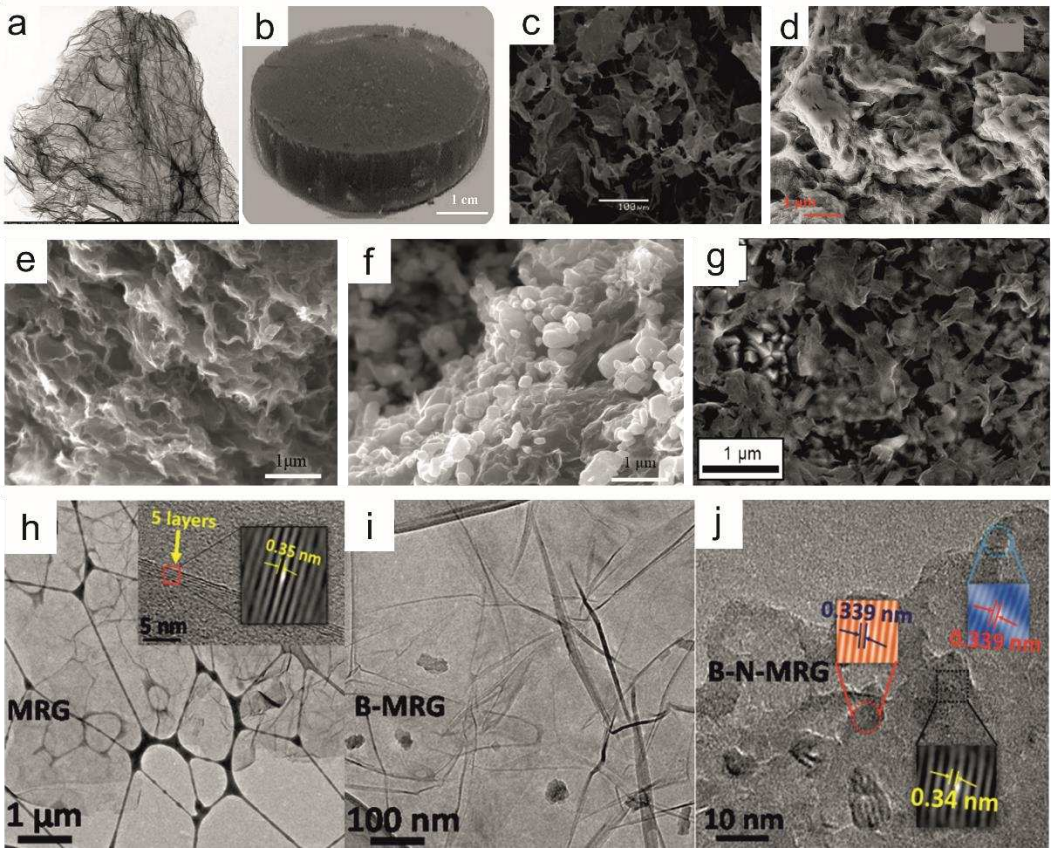

Figure 5. SEM image of (a) functionalized graphene [115]. (b) Photograph of gelatin-GO aerogel [152] and (c) SEM image of gelatin-GO aerogels $G_{10}GO_3$ [152]. SEM images of (d) 1:1.5NSG [88], (e) prGO (GO:ZnO=1:4) [117], (f) rGO/ZnO (GO:ZnO=1:4 (without HCl)) composites [117], (g) S-rGO-0.25 [116]. Reprinted with the permission from Elsevier, Refs. [115–117,152]. (h-j) TEM images of (h) MRG, (i) B-MRG, and (j) HRTEM image of B-N-MRG, Reprinted with the permission from American Chemical Society, Ref. [77]. .

MW radiation can easily be adapted to modify the graphene structure so that the carbon atoms in the graphene layer are replaced with other heteroatoms, such as N, S, P, or B [82,88,116] (please see Table 2). Interesting example was presented by Deepak K. Pattanayak and coworkers in 2020 (Figure 5d) [88]. A facile and one-pot MW-assisted synthesis resulted in doping of graphene with nitrogen and sulfur atoms (N,S-GO). Due to a superior amount of heteroatoms content (14.9% of N and 4.3% of S) in the graphene, the obtained material shows C_S of 310 F/g in two electrodes symmetric configuration using 1 M H_2SO_4 electrolyte. N,S-GO was also used in non-aqueous organic and ionic liquid electrolytes, where N,S-GO shows C_S of 226 F/g and 150 F/g with an energy density of 32 Wh/kg, respectively. The explanation of the heteroatom-doped graphene layer and the effect on the change of physical properties are described in detail in paragraph 3. Here we will limit ourselves to discussing only some interesting literature examples of the preparation of this type of doped structure.

Doping heteroatoms are an effective way to modify the physical properties of rGO. The modification of rGO using MW-assisted synthesis was applied to prepare S-doped rGO with different concentrations of sulfur (Figure 5g) [116]. The synthesis was performed in mild experimental conditions; at 140°C for 30 min, which led to the wrinkling and folding of graphene sheets. The material with the highest content of sulfur shows the excellent electrochemical performance. A five-fold increase in the number of sulfur atoms in the graphene sheets leads to an increase in the value from 61.7 to 237.6 F/g. With simultaneous high electrochemical stability, a capacitance retention of 106% after 10,000 cycles; the synthesized material has a promising potential for supercapacitor applications.

MW-assisted synthesis was also used to prepare B- and N-doped; and B, N-co-doped rGO (Figs. 5h-5j) [77]. The synthesized material possesses electromagnetic interference (EMI) shielding properties and high electrical conductivity. B,N-doped rGO shows high electrical conductivity compared to other materials: rGO, N-doped rGO and B-doped rGO, which results in better EMI shielding ability. A high EMI shielding of −42 dB (~99.99% attenuation) for B,N-doped rGO was measured compared to undoped rGO (−28 dB). The electrical conductivity increases from 21.4 (rGO) to 124.4 S/m (B, N-co-doped rGO) due to the nano junction inside the material. Their temperature-dependent electrical conductivity follows 2D-variable range hopping and Efros–Shklovskii-VRH conduction model in a low-temperature range ($T < 50$ K).

ND powders with different average particle sizes (from 10 nm to 1 μm) are sensitive to MWs between 2.49 and 9.43 GHz [153]. Increased permittivity with decreasing particle size, polarization and MW loss has already been observed. The oxygenation and hydrogenation *of the NDs* (sp^2-hybridization was raised in the sample) led to dielectric polarization, and the loss increased [105]. Various methods have been applied to increase the heating rate further and induce demanding reaction conditions. For example, specific substances, coating (MW-transparent substrates) or triggers have been added to tune the reaction conditions [101,103,105]. Using NDs in the environment of conducting polymers (ND-polyaniline) in MW-assisted synthesis significantly enhanced the MW absorption due to additional and intense polarization originating from the HN-CO groups acting as asymmetric centers [106]. These studies showed that ND particles might be applied as MW absorbers in MW-assisted heating. In some cases, such synthesis may require the addition of easily polarizing substances to tune the reaction conditions and to increase temperature.

MW-assisted synthesis was also applied for the preparation of onion-like structures the heavy crude oil and carbon catalyst (activated carbon and NiO-MoO_3/γ-Al_2O_3; 1:1 w/w) and tomatoes/carrots as a source of carbon and 30% NaOH [154,155]. The obtained CNs were non-homogenous with structural imperfections and an empty core; their structure did not resemble ND-derived CNOs.

The MW-assisted method was also successfully used to prepare and modify other CNs. An IL-assisted splitting method using MW irradiation as an external energy source produced graphene nanoribbons from MWCNT or SWCNT [156]. The process was based on two strategies: oxidation with strong acids and reduction with hydrazine. The MW-assisted method leads to splitting and expanding tubular graphite nanofibers, which consequently results in the preparation of graphene nanoribbons in the hundred nanometers. The MW-assisted synthesis was employed to prepare CNTs from acetylene and hydrogen as precursor gases [119]. The CNTs were tested for their ability to remove the crystal violet dye. The sorption capacity of CNTs was optimized on the adsorption process through response surface methodology. It was found that the sorption capacity was 81% at a pH value of 7.0 with 10 mg/L and a contact time of 25 min.

Using MW irradiation, it was possible to modify the tube walls in such a way as to remove the capped parts of the CNTs [54]. MW irradiation led to the opening of the nanotubes and the removal of fragments of the outer layers of CNTs. Moreover, it led to the formation of *sp3*-hybridized defects in the nanostructure. The morphology of CNTs was controlled by adjusting MW powers. The thinned and open-ended structure of CNTs can facilitate electron tunneling through barriers, and the wall's defects can serve as new active emission sites.

MW-assisted synthesis was applied to grow N-doped carbon quantum dots (N-CQDs) on the surface of MWCNTs [120]. In conventional methods, N-CQDs are incorporated into the MWCNT surface by multistep processes, including synthesis of the N-CQDs, their complex purification, surface activation, and crosslinking with the MWCNT surface. Using MW irradiation, the method is simplified by direct MW-assisted growth of NCQDs on the MWCNT surface. Additionally, this method of surface modification of MWCNTs effectively modulated their surface reactivity and internal band structure, which has a significant impact when studying electrocatalytic and photovoltaic processes. The dye-sensitized solar cells based on N-CQDs/MWCNTs, as a counter electrode, showed 50% higher photovoltaic performance as compared to pristine MWCNTs.

Preprints (www.preprints.org) | NOT PEER-REVIEWED | Posted: 3 August 2023 doi:10.20944/preprints202308.0283.v1

MW irradiation was applied to synthesizing composite containing GO and graphitic carbon nitride (g-C_3N_4), showing photocatalytic activity [121]. The enhanced photocatalytic activity of GO/g-C_3N_4 is the result of the ability of GO to accept and transport electrons from excited g-C_3N_4, which promotes charge separation. The GO/g-C_3N_4 photocatalysts possessed enhanced activities for H_2 production than pure g-C_3N_4 under visible light irradiation. The GO/g-C_3N_4 photocatalysts can reach a H_2-production rate of 224.6 μmol/h, a value nearly 12 times higher than those obtained for pristine g-C_3N_4. The studies show a promising potential of this nanocomposite for an electron collectors in photocatalytic hydrogen production.

An example of MW irradiation is presented at Gengchao Wang et al. [122], where N-doped porous graphene frameworks were synthesized. It is another example of creating a composite consisting of graphene and CQDTs. An N-doped porous graphene framework is synthesized quickly during several processes running simultaneously. A readily dispersible graphene was an effective receptor for MW absorption and initiated GO reduction. Next, the reduced part of GO, as an MW absorbing receptor, results in a reduction of the chain and allows N-doped porous graphene frameworks formation. The synthesized material possess a very good electrochemical performance and a volumetric absorption capacity which presents potential application value in catalysis, energy storage, and environmental protection (Table 2). The electrodes made of GO/g-C_3N_4 delivered a volumetric energy density of 12.3 mWh/cm^3 at a power density of 0.42 W/cm^3. The N-doped porous graphene frameworks exhibited extremely high volumetric absorption capacity of 100–243 g/cm^3 for different oils and organic solvents.

These studies showed that CNs might be applied as MW absorbers in MW-assisted synthesis. In some cases, such synthesis may require the addition of easily polarizing substances to tune the reaction conditions and to increase temperature. Optimizing these parameters allows for the synthesis or modification of the CNs quickly.

4.3. MW-assisted synthesis for the preparation of hybrid materials containing defective CNs: implications on properties and applications

MW irradiation is also a precious energy source for the preparation of multicomponent systems, often when conventional synthesis is highly complicated due to its multi-stage nature, product purification or time-consuming. In addition, it is possible to carry out the synthesis in different experimental conditions, such as, in the presence of a solvent or the solid phase, in ionic liquids or using materials of various origins, including inorganic and organic. Combining materials into larger supramolecular systems or composites is simple, with little time and energy consumption.

An ultrafast MW process allows synthesizing a carbon composite with the ordered mesoporous carbon as the core and CNT as the shell [151]. A 10–30 seconds MW irradiation catalyzed *in-situ* CNTs growth within the nanochannel of ordered mesoporous carbon. The whiskers morphology of the obtained composite looks like a rambutan. Such interconnection between CNTs and mesoporous carbon particles effectively bridges 3D conducting networks, promoting ion adsorption and diffusion of the supporting electrolyte. The preparation of a composite consisting of a copolymer and CNTs was also performed [128]. The oxidized CNTs were incorporated into the polymer matrix consisting of poly(*o*-phenylenediamine-co-aniline) using MW irradiation (for 45 min at intervals of 5 min) to accelerate the polymerization. The oxidation of CNTs was also supported by MW irradiation for 30 min at 160°C. The combining of these synthetic procedures led to the preparation of a composite with a needle-like structure of the copolymer. The structure of the copolymer and nanocomposite enables the effective accumulation of electric charge. They exhibited a high C_S of 147.14 F/g at 0.50 A/g with a capacitance retention of 82%.

MW irradiation is more often used to combine materials of different chemical nature, mainly for the synthesis of composites containing CNs and metallic nanoparticles [124,129,138,139,144,147,149], nanopellets [148] or core-shell structures [125–127]. Metallic nanoparticles can, of course, consist only of pristine metallic nanoparticles [147,150]; they can form metallic connections of various elements [125,126], metal hydroxide [132], metal oxides [130,157], nitride [142] or sulfides [129,146], in various combination, etc.

Preprints (www.preprints.org) | NOT PEER-REVIEWED | Posted: 3 August 2023 doi:10.20944/preprints202308.0283.v1

Since then, the world-wide studies of electrocatalytic processes have been dominated by precious-metal-based-materials: Pt-, Pd-, Mo-, Fe- and Co-based catalysts for ORR and HER [158–160]. Au- and Ag-based catalysts for electrocatalytic CO_2 reduction reaction (CO_2RR) [161,162], and Ru- and Ir-based catalysts for OER [163,164]. Generally, metal-based catalysts are characterized by low selectivity, poor durability and susceptibility to gas poisoning. Due to the cost and the scarcity of some metals, their practical and large-scale using is still limited. Pt nanoparticles have long been regarded as the best catalyst for ORR. However, due to its notable disadvantages listed above, the commercialization of these technologies is hampered. Therefore, it is necessary to search for alternative earth-abundant materials. CNs demonstrate excellent electrocatalytic activity with high stability [31,41,165]. A new generation of electrocatalysts is developed, in which multiple-proton-coupled electron transfer and mass transportation is promoted by defective surface of materials [35]. In this context, combining materials of the different chemical nature can optimize the properties of the designed materials.

The idea of using MW irradiation in composite preparation containing metallic nanoparticle and CNTs is schematically presented in Figure 6. In the first stage, CNs with metallic precursors and substances that are good MW absorbers are placed simultaneously in an MW reactor (Figure 6a). Graphene platelets in ionic liquids and palladium acetate were mixed in this case. Impregnation and partial exfoliation of graphene happened due to MW irradiation and weak van der Waal's and π-π interaction. The ionic liquid reduced the diameter of dissolved Pd cations. As a result, they created Pd nanoparticles, which were distributed on graphene sheets. At the same time, structural defects are formed in the graphene layer due to MW irradiation or the catalytic activity of the ionic liquid. These defects act as nucleation sites for core-shell structures of the Pd nanoparticles with imidazolium shells. During further MW irradiation, the outer organic layer decomposes, resulting in it being formed carbonaceous gasses. These are carbon sources for CNT growth. Carbon diffuses on the Pd nanoparticle's surface and comprises multi-walled core-shell nanoparticles.

It has to be noted that direct bonding between CNTs and graphene was detected due to the defect-based growth mechanism (Figure 6b). Under these conditions, we get a dense brush of CNTs with Pd nanoparticles placed perpendicularly to the graphene surface (Figure 6d). By manipulating the amount of graphene used for Pd and MW irradiation power and time, we can also quantitatively control the composition of the resulting hybrid material (Figure 6e). It is one of the most exciting literature examples of using MW irradiation to obtain hybrid materials. In many cases, it is simplified, mainly when we want to get two-component composites with a random 3D organization. This type of functionalization was presented in works, in which the carbonaceous component was graphene [147] and N-doped GO [144]. This process is illustrated in detail in Figure 3 and discussed in paragraph 4.2. Briefly, in multi-stage MW-assisted reactions, the agglomerated Pd nanoparticles (diameters of ~10 nm) create physical nanoholes in the graphene sheets. In contrast, much smaller Pd nanoparticles are incorporated inside graphene layers and bonded to graphene surfaces (Figure 4, Panel (II)) [147]. The composite is assigned as a nanohole-structured and Pd-embedded 3D porous graphene (3D Pd-E-PG) (Figure 4, Panel (II)). The results show that the 3D Pd-E-PG nanostructure has a ~5.4 wt % hydrogen storage capacity under 7.5 MPa and CO oxidation catalytic activity at 190 °C. The synthesized N-GO/Pd material was also used as catalysts for electrooxidation of ethanol with current density of 10 mA/cm^2 [144]. Analogous N-rGO/Pd material was used in direct-ethanol fuel cells [145]. The electrocatalytic activity of N-rGO/Pd was accessed by cyclic voltammetry in the presence of ethanol. The N-rGO/Pd catalyst exhibit better electrocatalytic performance than rGO/Pd, with electroactive surface area of 6.3 m^2/g and ~3.7 m^2/g, respectively.

Preprints (www.preprints.org) | NOT PEER-REVIEWED | Posted: 3 August 2023 doi:10.20944/preprints202308.0283.v1

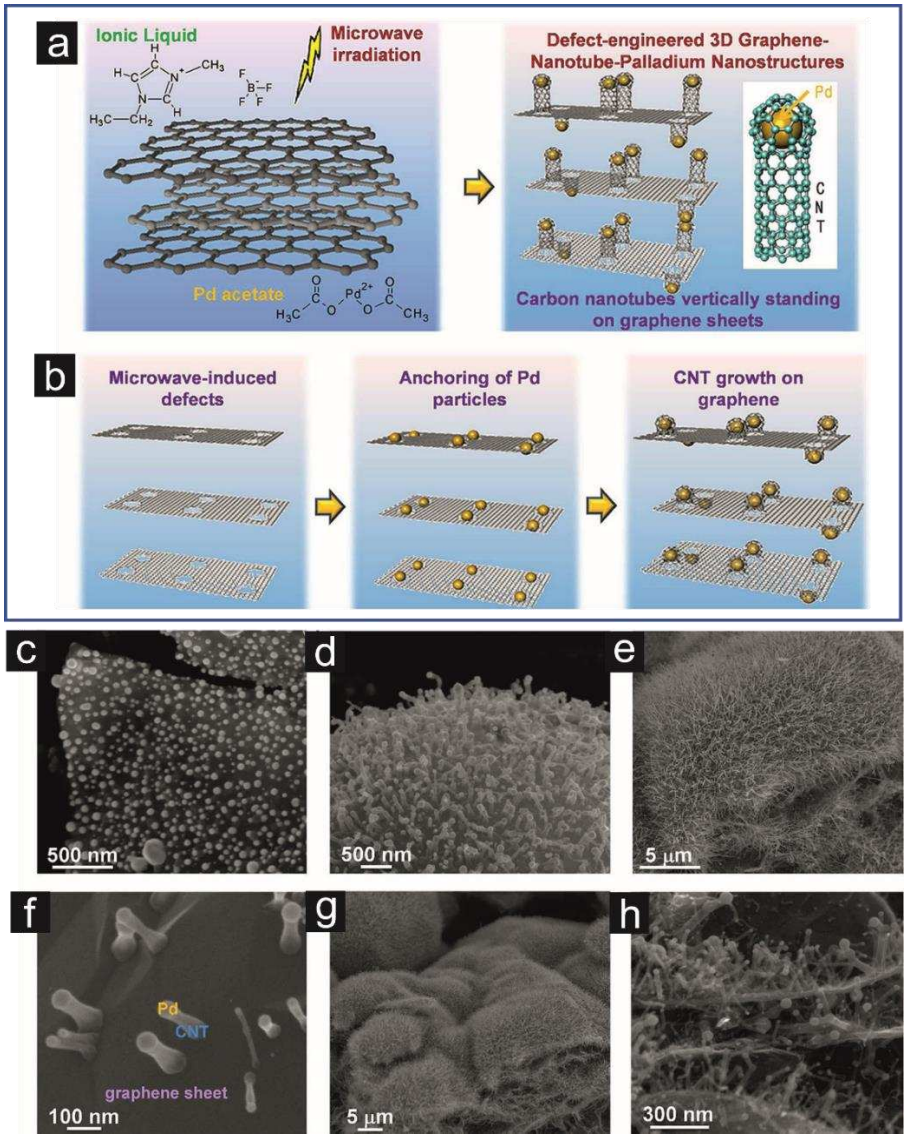

Figure 6. Schematic representation of one-pot MW synthesis of 3D carbon hybrid nanostructures showing vertically grown CNTs on graphene sheets: (a) scheme and (b) mechanism. (c-h) SEM images of 3D CNs showing CNTs vertically attached to graphene sheets: (c) Pd nanoparticles initially anchored on a graphene, (d) vertically standing CNTs grown on graphene by Pd nanoparticles, (e) CNT forest extensively grown on graphene surfaces after lengthy MW irradiation, (f) direct bonding between CNTs and graphene, (g) mass production of 3D G-CNT-Pd nanostructures, and (h) terrace structures of hybrid material. Reprinted with the permission from American Chemical Society, Ref. [150].

In addition to composites containing pure metallic nanoparticles, bimetallic nanoparticles or other compounds containing a metallic component are often synthesized. To the most common, it may include metal oxides [124,130,132,138,139,157], nitride [142] or sulfides [129,146], in various combinations, etc. MW-assisted synthesis is an effective method for the facile and fast preparation of hybrid materials. It is usually the last stage of the synthesis, often preceded by obtaining CNs or their initial modification.

A good example is an article on preparing a composite containing MWCNTs and Fe_3O_4 [124]. The pristine MWCNTs and N-doped MWCNTs were drilled through the chemical vapor deposition (CVD) method. Next, the Fe_3O_4 nanoparticles, with diameters between 5-15 nm, were synthesized directly on the MWCNT surface in an MW-assisted process. The homogeneous distribution of nanoparticles on the surface of CNs, formation of defects on the surface of MWCNTs during MW

irradiation and doping of CNs with nitrogen improve the saturation magnetization of the resulting composites.

An MW irradiation was also used as an energy source to support the preparation of NiO [132], $MnCo_2O_4$ [138], and α-MoO_3 [139,143]. Nanoparticles of metallic oxides were directly grown on graphene sheets using *in situ* MW irradiation method. A periodic repetition of MW irradiation through several cycles significantly increases the efficiency of the synthesis reaction leading to large-scale processes [143]. Multi-step preparation of sulfides [129,137,148,149] may also be simplified by using MW-hydrothermal preparation of nanoparticles. In this case, it is not necessary to use chemical surfactants, and the preparation time is significantly reduced from several days even to a few minutes. The homogenous distribution of CNs in solution was preceded by partial exfoliation of graphene, which was carried out by MW irradiation. This approach ensured a homogeneous distribution of nanoparticles in the bulk of the composite. The nanoparticles were covered with graphene sheets or intercalated inside the materials. It, in turn, provides a conductive scaffold constructed from graphene sheets, increasing the material's specific surface area and chemical stability. Hybrid composites' porous and interconnected structures promote charge transport by encapsulating agglomerated metallic nanoparticles.

Using MW irradiation, it is also possible to obtain core-shell structures quickly [125–127]. In this case, the CNTs, are surrounded by an inorganic phase, as shown in Figure 7a-d [125]. Briefly, in the first step, the oxidation of the MWCNTs was performed to increase their dispersibility and to introduce the nucleation sites for the inorganic nanoparticle creation. Next, a mixture of inorganic salt and an oxidizing agent was subjected to MW irradiation at elevated temperatures. Consequently, the walls of the MWCNTs were uniformly covered with an inorganic crystalline phase of various forms of crystallites. Depending on the irradiation power, temperature or reaction time, the degree of coverage of MWCNTs varied.

It is also possible to obtain a core-shell structure in the inorganic phase alone (Figure 7f-i). Then two phases with different crystal structures are distinguished [126]. A $CoMoO_4$ nanopellets have a core-shell form with a well-crystallized bulk. The shell of $CoMoO_4$ crystallite is amorphous. In both cases, the oxidized CNTs were utilized as MW absorbers and heterogeneous nucleation sites for inorganic nanocrystals formation. The MWCNT/$CoMoO_4$ composite shows a promising C_S of 170 F/g with a potential window of 0.8 V and a cycling stability of 93.2% after 1,000 cycles [126].

The CNT/$NiMn_2O_4$ composite synthesized by a MW-assisted hydrothermal process exhibited excellent electrochemical performance [125]. The electrochemical studies performed for this materials is shown in Figure 8. Briefly, the CNT/$NiMn_2O_4$ electrode exhibits a high C_S up to 915.6 F/g at 1 A/g and an excellent cycling stability of 93.0% after 5,000 cycles at 5 A/g. This properties are affected by the weaker crystallinity of $NiMn_2O_4$ and more defects and vacancies in CNTs. As shown in Figure 7c, the CV curves exhibit similar the electrochemical characteristic in the potential window from 1.3 to 1.6 V. An increasing of the voltage window, up to 1.7 V, results in current leap of charge due to the oxygen and/or hydrogen evolution reaction. The charge-discharge (GCD) curves show good linearity and symmetry within 1.3-1.6 V potential windows at 1.5 A/g (Figure 8d). An asymmetric supercapacitor device with a positive electrode composed from CNT/$NiMn_2O_4$ shows the maximum energy density of 36.5 Wh/kg at a power density of 800 W/kg and a cycling stability of 82.8% after 10,000 cycles at 5 A/g (Figure 8i). This parameters are higher than for other supercapacitor devices based on NiMn.

Preprints (www.preprints.org) | NOT PEER-REVIEWED | Posted: 3 August 2023 doi:10.20944/preprints202308.0283.v1

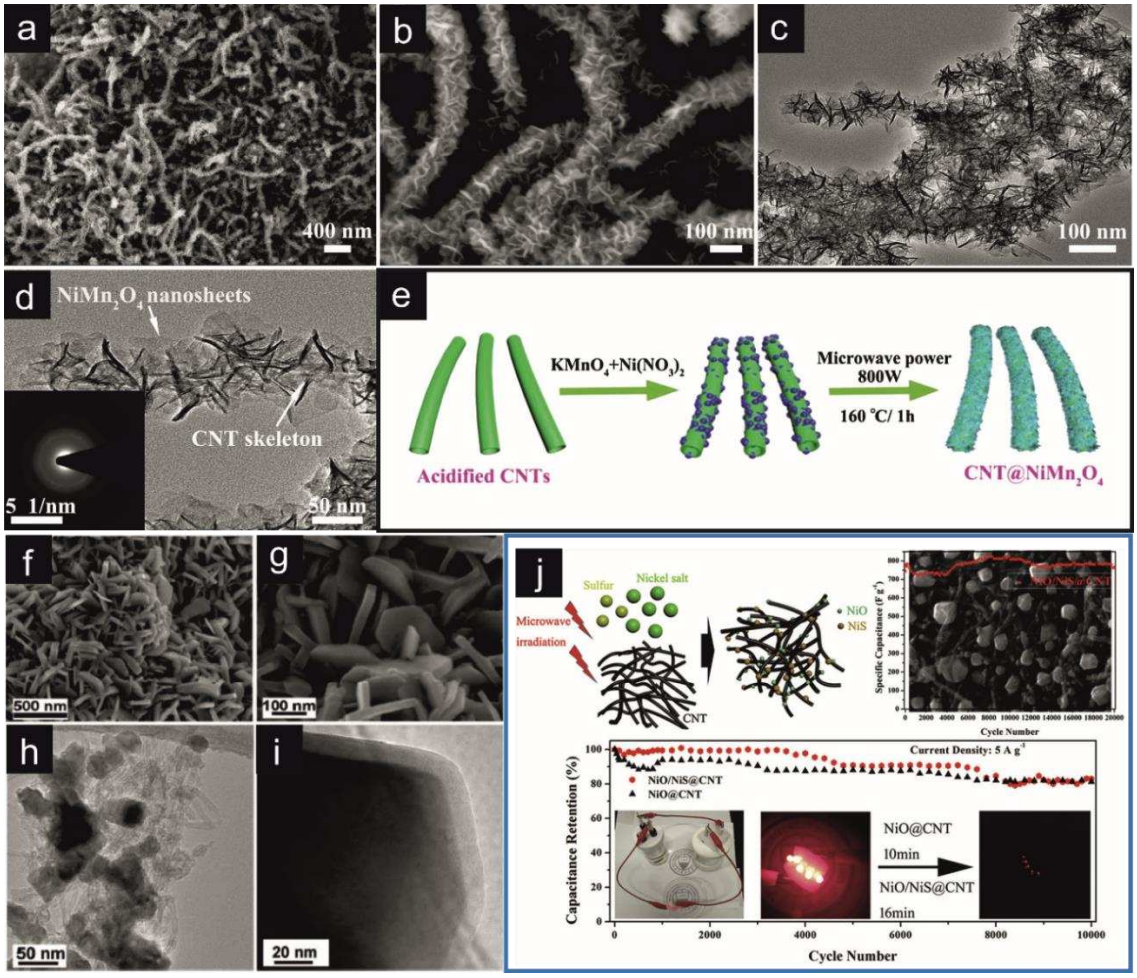

Figure 7. Schematic representation of the core-shell structures prepared by MW-assisted synthesis. (a,b) The low and high magnification of FESEM images of CNT/$NiMn_2O_4$ composite (c,d) TEM images of CNT/$NiMn_2O_4$ composite; inset shows the selected area electron diffraction pattern. (e) Schematic representation of the formation of core-shell structures of the CNT/$NiMn_2O_4$ composite. Reprinted with the permission of Elsevier from Ref. [125]. (f,g) SEM and (h) BF TEM images of MWCNT/$CoMoO_4$. (i) TEM image of individual $CoMoO_4$ crystallite (core-shell structure). Reprinted with the permission from RSC, Ref. [126]. (j) Schematic illustration of the formation of NiS@CNT/NiO nanocomposites. SEM image of NiS@CNT/NiO. Cycling stability of the ASC (five red LED indicators were successfully lit). Reprinted with the permission from Elsevier, Ref. [127].

A multi-component nanocomposite consisting of CNTs, NiO and NiS (NiS@CNT/NiO) was prepared quickly (60 s) using a one-step MW-assisted method (please see Table 2, Figure 7j) [127]. The electrochemical performances of the electrodes were studied concerning different mass ratios of used substrates and MW conditions performed reaction. The composites containing both inorganic components: NiS and NiO, showed optimal electrochemical performance. The NiS@CNT/NiO electrodes showed a C_S of 809.7 F/g at 1 A/g and a cycling stability of approximately 100% retention after 20,000 cycles at 5 A/g. In the following example, MW-assisted hydrothermal synthesis was also used to prepare the composite containing NiS and rGO (rGO/NiS) [129]. Compared to the conventional multi-step preparation process, the MW-assisted synthesis eliminates chemical surfactants and reduces the preparation time from several days to only 6 h [129]. The electrodes fabricated from rGO/NiS exhibits a ultrahigh C_S of 1745.7 F/g at 1 A/g and a high capacity retention after 3,000 cycles with high reproducibility.

Preprints (www.preprints.org) | NOT PEER-REVIEWED | Posted: 3 August 2023 doi:10.20944/preprints202308.0283.v1

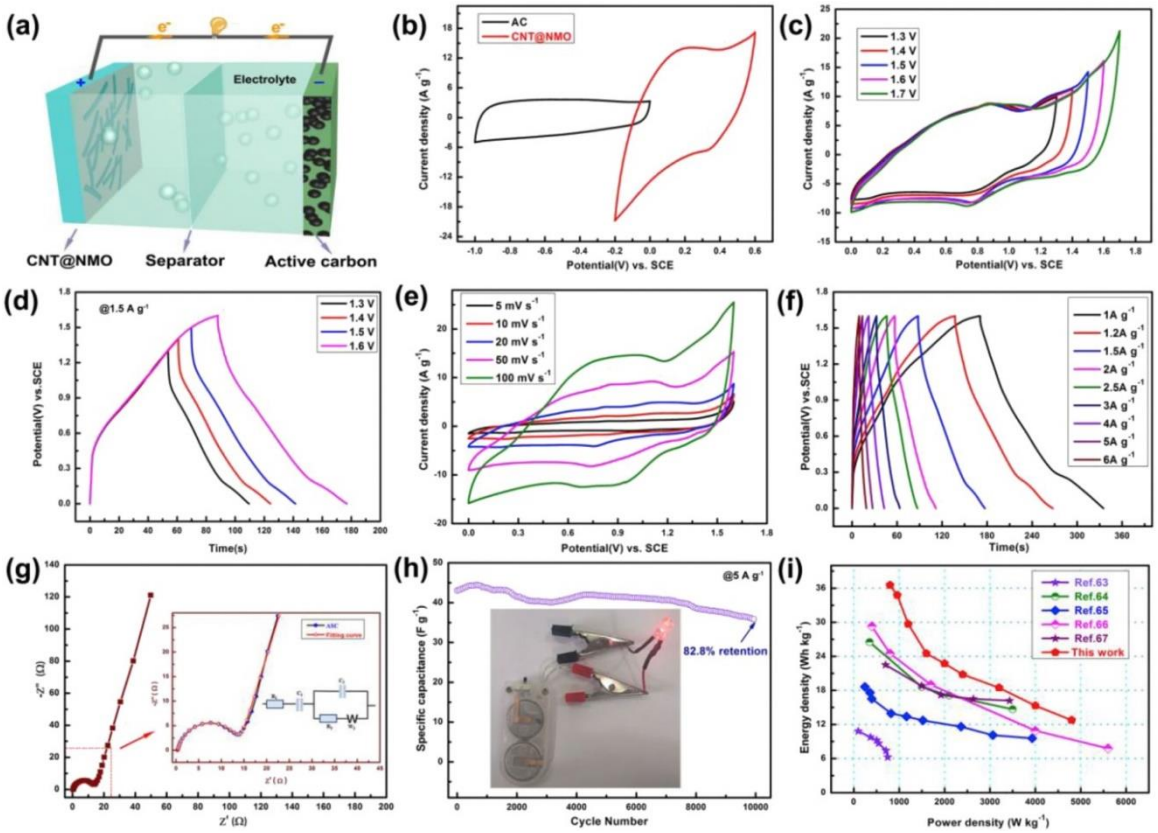

Figure 8. (a) Schematic diagram of CNT/$NiMn_2O_4$ asymmetric supercapacitor device. (b) Comparative CV curves of AC CNT/$NiMn_2O_4$ electrodes in a three-electrode system, 50 mV/s. (c) CVs of the device measured at different potential window, 50 mV/s. (d) GCD curves of the device measured at different potential window at 1.5 A/g. (e) CVs at the different scan rates from o to 1.6 V. (f) GCD curves measured at different current densities. (g) EIS spectra of device. (h) Cyclic performance of the device at 5 A/g for 10,000 cycles. (i) The Regone plots of the CNT/$NiMn_2O_4$ and comparison with literature data. Reprinted with the permission from Elsevier, Ref. [125]. .

The symmetric solid-state supercapacitor shows a C_S of 14.20 F/g, an energy density of 7.1 Wh/kg and a power density of 1836 W/kg. The supercapacitor device based on N-rGO/NiS exhibit similar electrochemical performance with a C_S of 1467.8 F/g at 1 A/g [137]. In an asymmetric configuration of N-rGO//N-rGO/NiS in 6 M KOH and graphite sheet as the current collector, the device shows a cyclic stability of 86.6% after 5,000 cycles, energy density of 66.6 Wh/kg at a power density of 405.83 W/kg. Due to their high energy and power density and excellent cycling stability, the hybrid materials show potential for energy-storage applications.

The 3D S-rGO/$NiFeS_2$ composite was synthesized by one-step MW alcohothermal method, in which mercaptoacetic acid is used as a sulfur source for doping of graphene and as precursor of nickel-iron sulfide [146]. The composite shows a very porous structure and a large specific surface area, and thanks to chemical bonds with sulfur, it increases the binding of the nickel-iron precursor to the carbon material. These phenomena ensure the C_S value of 643.9 C/g (1073.2 F/g) at the current density of 1 A/g in 6.0 M KOH electrolyte. The asymmetric supercapacitor device delivers a energy density of 45.7 Wh/kg at a power density of 222 W/kg under a wide potential range of 1.6 V. Due to high energy and power density and excellent cycling stability, the hybrid materials containing carbon nanostructures and Ni component show potential for energy-storage applications.

Simonkolleite ($Zn_5(OH)_8Cl_2{\cdot}H_2O$) nanoplatelets were deposited on nickel foam-supported graphene (NiF-G/SimonK) using an MW-assisted hydrothermal method [148]. In this condition, the porous NiF-G/SimonK composite was obtained, in which the structural and morphological characteristic significantly affects the electrochemical performance. The NiF-G/SimonK composite,

 doi:10.20944/preprints202308.0283.v1

used as electrodes, exhibits a C_S of 836 F/g at a current density of 1 A/g and a cycling stability with capacitance retention of 92% after 5,000 charge/discharge cycles. An MW-assisted synthesis was used to prepare honeycomb-like graphene/NiCoS (G/NiCoS) composite [149]. The defect-rich structures of G/NiCoS ensure excellent electrochemical properties of this composite. The device with the electrodes made of G/NiCoS exhibit a high C_S of 1186 F/g at 1 A/g and a capacity of 89.2% after 10,000 cycles, and an energy density of 46.4 Wh/kg.

Due to their high energy and power density and excellent cycling stability, the multi-component hybrid materials show potential for energy-storage applications and electrocatalysis.

5. Concluding Remarks

The electrochemical properties of carbon-based electrode materials are closely related to their chemical composition, structure and defects. They are ideal for catalysis, electrocatalysis and electrochemistry due to their excellent conductivity and mechanical stability, large specific area with microporosity, easy production of defective motifs in their structures and high charged carrier mobility. They are also good candidates for electrocatalysis due to the easy formation of the defects in their networks that affect decreasing the reaction kinetic barriers while simultaneously increasing the efficiency and selectivity of the chemical transformation involved. From a chemical point of view, the essence of catalysis is breaking and re-forming chemical bonds under the influence of an external force. A simple carbon-carbon or carbon-heteroatom bond formation can produce fuels (H_2 and O_2) using green chemistry processes. Since all these parameters are easily achievable during the creation or modification of CNs during MW irradiation, it has recently become an increasingly used method. It was not only the simplicity, reaction time and the possibility of conducting it both in solution and in the solid phase that decided about it, but mainly the possibility of combining substrates of different chemical natures. Despite the many advantages of CNs, in some cases, it is necessary to combine them with an inorganic component. Here, too, an MW irradiation is an excellent source of energy that activates the course of a chemical reaction between organic and inorganic phases.

In our review, we indicated that it is possible to create multi-component materials thanks to MW-assisted synthesis. Not only is it easy and quick to combine inorganic and carbonaceous materials, but often the resulting materials exhibit unique structures and morphologies that need to be more attainable using conventional methods. Their physical and chemical properties make it possible to use them in many scientific fields. Here, we focused mainly on the electrochemical and electrocatalytic properties of the obtained materials because, in these areas, new solutions are constantly being sought that will enable the production of nanodevices with the optimal parameters. Unfortunately, many of the solutions presented here still need to meet the parameters desired on an industrial scale. Despite this, the examples of creating hybrid materials with MW irradiation presented here have great potential, and this trend should be developed in the future.

Author Contributions: Conceptualization, M.E.P.-B.; writing—original draft preparation, D.P. and M.E.P.-B.; writing—review and editing, M.E.P.-B.; visualization, D.P. and M.E.P.-B.; supervision, M.E.P.-B.; project administration, M.E.P.-B.; funding acquisition, M.E.P.-B. The authors have read and agreed to the published version of the manuscript.

Funding: We gratefully acknowledge the financial support of the National Science Centre, Poland, grant #2019/35/B/ST5/00572 to M.E.P.-B.

Institutional Review Board Statement: Not applicable.

Informed Consent Statement: Not applicable.

Conflicts of Interest: The authors declare no conflict of interest.

References

1. Yu, S.-S.; Zheng, W.-T. Effect of N/B Doping on the Electronic and Field Emission Properties for Carbon Nanotubes, Carbon Nanocones, and Graphene Nanoribbons. *Nanoscale* **2010**, *2*, 1069, doi:10.1039/c0nr00002g.

2. Rathinavel, S.; Priyadharshini, K.; Panda, D. A Review on Carbon Nanotube: An Overview of Synthesis, Properties, Functionalization, Characterization, and the Application. *Mater. Sci. Eng. B* **2021**, *268*, 115095, doi:10.1016/j.mseb.2021.115095.
3. Robertson, J. Comparison of Diamond-like Carbon to Diamond for Applications. *Phys. Status Solidi A* **2008**, *205*, 2233–2244, doi:10.1002/pssa.200879720.
4. Robertson, J. Electronic Structure of Diamond-like Carbon. *Diam. Relat. Mater.* **1997**, *6*, 212–218, doi:10.1016/S0925-9635(96)00627-9.
5. Mykhailiv, O.; Zubyk, H.; Plonska-Brzezinska, M.E. Carbon Nano-Onions: Unique Carbon Nanostructures with Fascinating Properties and Their Potential Applications. *Inorganica Chim. Acta* **2017**, *468*, 49–66, doi:10.1016/j.ica.2017.07.021.
6. Yang, G.; Li, L.; Lee, W.B.; Ng, M.C. Structure of Graphene and Its Disorders: A Review. *Sci. Technol. Adv. Mater.* **2018**, *19*, 613–648, doi:10.1080/14686996.2018.1494493.
7. Gao, X.; Liu, H.; Wang, D.; Zhang, J. Graphdiyne: Synthesis, Properties, and Applications. *Chem. Soc. Rev.* **2019**, *48*, 908–936, doi:10.1039/C8CS00773J.
8. Khan, K.; Tareen, A.K.; Iqbal, M.; Shi, Z.; Zhang, H.; Guo, Z. Novel Emerging Graphdiyne Based Two Dimensional Materials: Synthesis, Properties and Renewable Energy Applications. *Nano Today* **2021**, *39*, 101207, doi:10.1016/j.nantod.2021.101207.
9. Zhao, Y.; Yang, N.; Yu, R.; Zhang, Y.; Zhang, J.; Li, Y.; Wang, D. Unique Structural Advances of Graphdiyne for Energy Applications. *EnergyChem* **2020**, *2*, 100041, doi:10.1016/j.enchem.2020.100041.
10. Liu, H.; Zhang, L.; Yan, M.; Yu, J. Carbon Nanostructures in Biology and Medicine. *J. Mater. Chem. B* **2017**, *5*, 6437–6450, doi:10.1039/C7TB00891K.
11. Hu, Y.; Shenderova, O.A.; Hu, Z.; Padgett, C.W.; Brenner, D.W. Carbon Nanostructures for Advanced Composites. *Rep. Prog. Phys.* **2006**, *69*, 1847–1895, doi:10.1088/0034-4885/69/6/R05.
12. Gu, W.; Yushin, G. Review of Nanostructured Carbon Materials for Electrochemical Capacitor Applications: Advantages and Limitations of Activated Carbon, Carbide-Derived Carbon, Zeolite-Templated Carbon, Carbon Aerogels, Carbon Nanotubes, Onion-like Carbon, and Graphene: Nanostructured Carbon Materials for Electrochemical Capacitor Applications. *Wiley Interdiscip. Rev. Energy Environ.* **2014**, *3*, 424–473, doi:10.1002/wene.102.
13. Al-Jumaili, A.; Alancherry, S.; Bazaka, K.; Jacob, M. Review on the Antimicrobial Properties of Carbon Nanostructures. *Materials* **2017**, *10*, 1066, doi:10.3390/ma10091066.
14. Bobrowska, D.M.; Olejnika, P.; Echegoyen, L.; Brzezinska, M. Onion-like Carbon Nanostructures: An Overview of Bio-Applications. *Curr. Med. Chem.* **2018**, *25*, doi:10.2174/0929867325666181101105535.
15. Kumar, S.; Rani, R.; Dilbaghi, N.; Tankeshwar, K.; Kim, K.-H. Carbon Nanotubes: A Novel Material for Multifaceted Applications in Human Healthcare. *Chem. Soc. Rev.* **2017**, *46*, 158–196, doi:10.1039/C6CS00517A.
16. Sek, S.; Breczko, J.; Plonska-Brzezinska, M.E.; Wilczewska, A.Z.; Echegoyen, L. STM-Based Molecular Junction of Carbon Nano-Onion. *ChemPhysChem* **2013**, *14*, 96–100, doi:10.1002/cphc.201200624.
17. Wang, M.-S.; Golberg, D.; Bando, Y. Carbon "Onions" as Point Electron Sources. *ACS Nano* **2010**, *4*, 4396–4402, doi:10.1021/nn1013353.
18. Keller, N.; Maksimova, N.I.; Roddatis, V.V.; Schur, M.; Mestl, G.; Butenko, Y.V.; Kuznetsov, V.L.; Schlögl, R. The Catalytic Use of Onion-like Carbon Materials for Styrene Synthesis by Oxidative Dehydrogenation of Ethylbenzene. *Angew. Chem. Int. Ed Engl.* **2002**, *41*, 1885–1888.
19. Su, D.; Maksimova, N.I.; Mestl, G.; Kuznetsov, V.L.; Keller, V.; Schlögl, R.; Keller, N. Oxidative Dehydrogenation of Ethylbenzene to Styrene over Ultra-Dispersed Diamond and Onion-like Carbon. *Carbon* **2007**, *45*, 2145–2151, doi:10.1016/j.carbon.2007.07.005.
20. Plonska-Brzezinska, M.E.; Echegoyen, L. Carbon Nano-Onions for Supercapacitor Electrodes: Recent Developments and Applications. *J. Mater. Chem. A* **2013**, *1*, 13703, doi:10.1039/c3ta12628e.
21. Luszczyn, J.; Plonska-Brzezinska, M.E.; Palkar, A.; Dubis, A.T.; Simionescu, A.; Simionescu, D.T.; Kalska-Szostko, B.; Winkler, K.; Echegoyen, L. Small Noncytotoxic Carbon Nano-Onions: First Covalent Functionalization with Biomolecules. *Chem. - Eur. J.* **2010**, *16*, 4870–4880, doi:10.1002/chem.200903277.
22. Breczko, J.; Plonska-Brzezinska, M.E.; Echegoyen, L. Electrochemical Oxidation and Determination of Dopamine in the Presence of Uric and Ascorbic Acids Using a Carbon Nano-Onion and Poly(Diallyldimethylammonium Chloride) Composite. *Electrochimica Acta* **2012**, *72*, 61–67, doi:10.1016/j.electacta.2012.03.177.
23. Huang, Y.; Liang, J.; Chen, Y. The Application of Graphene Based Materials for Actuators. *J. Mater. Chem.* **2012**, *22*, 3671, doi:10.1039/c2jm15536b.
24. Banerjee, A.N. Graphene and Its Derivatives as Biomedical Materials: Future Prospects and Challenges. *Interface Focus* **2018**, *8*, 20170056, doi:10.1098/rsfs.2017.0056.
25. Bartelmess, J.; Giordani, S. Carbon Nano-Onions (Multi-Layer Fullerenes): Chemistry and Applications. *Beilstein J. Nanotechnol.* **2014**, *5*, 1980–1998, doi:10.3762/bjnano.5.207.

26. Ghosh, M.; Sonkar, S.K.; Saxena, M.; Sarkar, S. Carbon Nano-Onions for Imaging the Life Cycle of Drosophila Melanogaster. *Small* **2011**, *7*, 3170–3177, doi:10.1002/smll.201101158.
27. Giordani, S.; Bartelmess, J.; Frasconi, M.; Biondi, I.; Cheung, S.; Grossi, M.; Wu, D.; Echegoyen, L.; O'Shea, D.F. NIR Fluorescence Labelled Carbon Nano-Onions: Synthesis, Analysis and Cellular Imaging. *J Mater Chem B* **2014**, *2*, 7459–7463, doi:10.1039/C4TB01087F.
28. Mykhailiv, O.; Brzezinski, K.; Sulikowski, B.; Olejniczak, Z.; Gras, M.; Lota, G.; Molina-Ontoria, A.; Jakubczyk, M.; Echegoyen, L.; Plonska-Brzezinska, M.E. Boron-Doped Polygonal Carbon Nano-Onions: Synthesis and Applications in Electrochemical Energy Storage. *Chem. - Eur. J.* **2017**, *23*, 7132–7141, doi:10.1002/chem.201700914.
29. Simon, P.; Gogotsi, Y. Materials for Electrochemical Capacitors. *Nat. Mater.* **2008**, *7*, 845–854, doi:10.1038/nmat2297.
30. Li, D.; Jia, Y.; Chang, G.; Chen, J.; Liu, H.; Wang, J.; Hu, Y.; Xia, Y.; Yang, D.; Yao, X. A Defect-Driven Metal-Free Electrocatalyst for Oxygen Reduction in Acidic Electrolyte. *Chem* **2018**, *4*, 2345–2356, doi:10.1016/j.chempr.2018.07.005.
31. Jiang, Y.; Yang, L.; Sun, T.; Zhao, J.; Lyu, Z.; Zhuo, O.; Wang, X.; Wu, Q.; Ma, J.; Hu, Z. Significant Contribution of Intrinsic Carbon Defects to Oxygen Reduction Activity. *ACS Catal.* **2015**, *5*, 6707–6712, doi:10.1021/acscatal.5b01835.
32. Tang, C.; Wang, H.-F.; Chen, X.; Li, B.-Q.; Hou, T.-Z.; Zhang, B.; Zhang, Q.; Titirici, M.-M.; Wei, F. Topological Defects in Metal-Free Nanocarbon for Oxygen Electrocatalysis. *Adv. Mater.* **2016**, *28*, 6845–6851, doi:10.1002/adma.201601406.
33. Banham, D.; Ye, S.; Pei, K.; Ozaki, J.; Kishimoto, T.; Imashiro, Y. A Review of the Stability and Durability of Non-Precious Metal Catalysts for the Oxygen Reduction Reaction in Proton Exchange Membrane Fuel Cells. *J. Power Sources* **2015**, *285*, 334–348, doi:10.1016/j.jpowsour.2015.03.047.
34. Zheng, Y.; Jiao, Y.; Zhu, Y.; Cai, Q.; Vasileff, A.; Li, L.H.; Han, Y.; Chen, Y.; Qiao, S.-Z. Molecule-Level g-C_3N_4 Coordinated Transition Metals as a New Class of Electrocatalysts for Oxygen Electrode Reactions. *J. Am. Chem. Soc.* **2017**, *139*, 3336–3339, doi:10.1021/jacs.6b13100.
35. Jia, Y.; Jiang, K.; Wang, H.; Yao, X. The Role of Defect Sites in Nanomaterials for Electrocatalytic Energy Conversion. *Chem* **2019**, *5*, 1371–1397, doi:10.1016/j.chempr.2019.02.008.
36. Yan, X.; Jia, Y.; Yao, X. Defects on Carbons for Electrocatalytic Oxygen Reduction. *Chem. Soc. Rev.* **2018**, *47*, 7628–7658, doi:10.1039/C7CS00690J.
37. Chung, H.T.; Cullen, D.A.; Higgins, D.; Sneed, B.T.; Holby, E.F.; More, K.L.; Zelenay, P. Direct Atomic-Level Insight into the Active Sites of a High-Performance PGM-Free ORR Catalyst. *Science* **2017**, *357*, 479–484, doi:10.1126/science.aan2255.
38. Deng, D.; Yu, L.; Pan, X.; Wang, S.; Chen, X.; Hu, P.; Sun, L.; Bao, X. Size Effect of Graphene on Electrocatalytic Activation of Oxygen. *Chem. Commun.* **2011**, *47*, 10016, doi:10.1039/c1cc13033a.
39. Liu, D.; Ni, K.; Ye, J.; Xie, J.; Zhu, Y.; Song, L. Tailoring the Structure of Carbon Nanomaterials toward High-End Energy Applications. *Adv. Mater.* **2018**, *30*, 1802104, doi:10.1002/adma.201802104.
40. Kotakoski, J.; Krasheninnikov, A.V.; Kaiser, U.; Meyer, J.C. From Point Defects in Graphene to Two-Dimensional Amorphous Carbon. *Phys. Rev. Lett.* **2011**, *106*, doi:10.1103/PhysRevLett.106.105505.
41. Yang, H.B.; Miao, J.; Hung, S.-F.; Chen, J.; Tao, H.B.; Wang, X.; Zhang, L.; Chen, R.; Gao, J.; Chen, H.M.; et al. Identification of Catalytic Sites for Oxygen Reduction and Oxygen Evolution in N-Doped Graphene Materials: Development of Highly Efficient Metal-Free Bifunctional Electrocatalyst. *Sci. Adv.* **2016**, *2*, e1501122, doi:10.1126/sciadv.1501122.
42. Jia, Y.; Chen, J.; Yao, X. Defect Electrocatalytic Mechanism: Concept, Topological Structure and Perspective. *Mater. Chem. Front.* **2018**, *2*, 1250–1268, doi:10.1039/C8QM00070K.
43. Yan, X.; Jia, Y.; Yao, X. Defects on Carbons for Electrocatalytic Oxygen Reduction. *Chem. Soc. Rev.* **2018**, *47*, 7628–7658, doi:10.1039/C7CS00690J.
44. Frauenheim, Th.; Blaudeck, P.; Stephan, U.; Jungnickel, G. Atomic Structure and Physical Properties of Amorphous Carbon and Its Hydrogenated Analogs. *Phys. Rev. B* **1993**, *48*, 4823–4834, doi:10.1103/PhysRevB.48.4823.
45. Cho, N.-H.; Krishnan, K.M.; Veirs, D.K.; Rubin, M.D.; Hopper, C.B.; Bhushan, B.; Bogy, D.B. Chemical Structure and Physical Properties of Diamond-like Amorphous Carbon Films Prepared by Magnetron Sputtering. *J. Mater. Res.* **1990**, *5*, 2543–2554, doi:10.1557/JMR.1990.2543.
46. Mounier, E.; Bertin, F.; Adamik, M.; Pauleau, Y.; Barna, P.B. Effect of the Substrate Temperature on the Physical Characteristics of Amorphous Carbon Films Deposited by d.c. Magnetron Sputtering. *Diam. Relat. Mater.* **1996**, *5*, 1509–1515, doi:10.1016/S0925-9635(96)00575-4.
47. Zhou, H.; Sheng, X.; Xiao, J.; Ding, Z.; Wang, D.; Zhang, X.; Liu, J.; Wu, R.; Feng, X.; Jiang, L. Increasing the Efficiency of Photocatalytic Reactions via Surface Microenvironment Engineering. *J. Am. Chem. Soc.* **2020**, *142*, 2738–2743, doi:10.1021/jacs.9b12247.
48. Bai, S.; Jiang, W.; Li, Z.; Xiong, Y. Surface and Interface Engineering in Photocatalysis. *ChemNanoMat* **2015**, *1*, 223–239, doi:10.1002/cnma.201500069.

49. Li, J.; Abbas, S.U.; Wang, H.; Zhang, Z.; Hu, W. Recent Advances in Interface Engineering for Electrocatalytic CO2 Reduction Reaction. *Nano-Micro Lett.* **2021**, *13*, 216, doi:10.1007/s40820-021-00738-9.
50. Chen, S.; Liu, X.; Xiong, J.; Mi, L.; Song, X.-Z.; Li, Y. Defect and Interface Engineering in Metal Sulfide Catalysts for the Electrocatalytic Nitrogen Reduction Reaction: A Review. *J. Mater. Chem. A* **2022**, *10*, 6927–6949, doi:10.1039/D2TA00070A.
51. Miller, J.R.; Simon, P. The Chalkboard: Fundamentals of Electrochemical Capacitor Design and Operation. *Electrochem. Soc. Interface* **2008**, *17*, 31–32, doi:10.1149/2.F02081IF.
52. Simon, P.; Gogotsi, Y. Perspectives for Electrochemical Capacitors and Related Devices. *Nat. Mater.* **2020**, *19*, 1151–1163, doi:10.1038/s41563-020-0747-z.
53. Liu, D.; Ni, K.; Ye, J.; Xie, J.; Zhu, Y.; Song, L. Carbon Nanomaterials: Tailoring the Structure of Carbon Nanomaterials toward High-End Energy Applications (Adv. Mater. 48/2018). *Adv. Mater.* **2018**, *30*, 1870371, doi:10.1002/adma.201870371.
54. Deng, J.-H.; Cheng, L.; Wang, F.-J.; Yu, B.; Li, G.-Z.; Li, D.-J.; Cheng, G.-A. Ultralow Field Emission from Thinned, Open-Ended, and Defected Carbon Nanotubes by Using Microwave Hydrogen Plasma Processing. *Appl. Surf. Sci.* **2015**, *324*, 293–299, doi:10.1016/j.apsusc.2014.10.137.
55. Ferrari, A.C.; Meyer, J.C.; Scardaci, V.; Casiraghi, C.; Lazzeri, M.; Mauri, F.; Piscanec, S.; Jiang, D.; Novoselov, K.S.; Roth, S.; et al. Raman Spectrum of Graphene and Graphene Layers. *Phys. Rev. Lett.* **2006**, *97*, 187401, doi:10.1103/PhysRevLett.97.187401.
56. Tuinstra, F.; Koenig, J.L. Raman Spectrum of Graphite. *J. Chem. Phys.* **1970**, *53*, 1126–1130, doi:10.1063/1.1674108.
57. Electron Emission in Intense Electric Fields. *Proc. R. Soc. Lond. Ser. Contain. Pap. Math. Phys. Character* **1928**, *119*, 173–181, doi:10.1098/rspa.1928.0091.
58. An, Y.; Li, C.; Sun, X.; Wang, K.; Su, F.; Liu, F.; Zhang, X.; Ma, Y. Deoxygenated Porous Carbon with Highly Stable Electrochemical Reaction Interface for Practical High-Performance Lithium-Ion Capacitors. *J. Phys. Appl. Phys.* **2022**, *55*, 045501, doi:10.1088/1361-6463/ac2db3.
59. Wang, C.; Chi, M.; Wang, G.; van der Vliet, D.; Li, D.; More, K.; Wang, H.-H.; Schlueter, J.A.; Markovic, N.M.; Stamenkovic, V.R. Correlation Between Surface Chemistry and Electrocatalytic Properties of Monodisperse PtxNi1-x Nanoparticles. *Adv. Funct. Mater.* **2011**, *21*, 147–152, doi:10.1002/adfm.201001138.
60. Trasatti, S. Oxide/Aqueous Solution Interfaces, Interplay of Surface Chemistry and Electrocatalysis. *Mater. Chem. Phys.* **1987**, *16*, 157–174, doi:10.1016/0254-0584(87)90027-7.
61. Chen, D.; Zou, Y.; Wang, S. Surface Chemical-Functionalization of Ultrathin Two-Dimensional Nanomaterials for Electrocatalysis. *Mater. Today Energy* **2019**, *12*, 250–268, doi:10.1016/j.mtener.2019.01.006.
62. Kumar, R.; Sahoo, S.; Joanni, E.; Singh, R.K.; Maegawa, K.; Tan, W.K.; Kawamura, G.; Kar, K.K.; Matsuda, A. Heteroatom Doped Graphene Engineering for Energy Storage and Conversion. *Mater. Today* **2020**, *39*, 47–65, doi:10.1016/j.mattod.2020.04.010.
63. Basivi, P.K.; Pasupuleti, K.S.; Gelija, D.; Kim, M.-D.; Pasupuleti, V.R.; Kim, C.W. UV-Light-Enhanced Room Temperature NO 2 Gas-Sensing Performances Based on Sulfur-Doped Graphitic Carbon Nitride Nanoflakes. *New J. Chem.* **2022**, *46*, 19254–19262, doi:10.1039/D2NJ04117K.
64. Fortunato, G.V.; Kronka, M.S.; Cardoso, E.S.F.; dos Santos, A.J.; Roveda, A.C.; Lima, F.H.B.; Ledendecker, M.; Maia, G.; Lanza, M.R.V. A Comprehensive Comparison of Oxygen and Nitrogen Functionalities in Carbon and Their Implications for the Oxygen Reduction Reaction. *J. Catal.* **2022**, *413*, 1034–1047, doi:10.1016/j.jcat.2022.08.001.
65. Szymański, G.S.; Wiśniewski, M.; Olejnik, P.; Koter, S.; Castro, E.; Echegoyen, L.; Terzyk, A.P.; Plonska-Brzezinska, M.E. Correlation between the Catalytic and Electrocatalytic Properties of Nitrogen-Doped Carbon Nanoonions and the Polarity of the Carbon Surface: Experimental and Theoretical Investigations. *Carbon* **2019**, *151*, 120–129, doi:10.1016/j.carbon.2019.05.069.
66. Zheng, Y.; Jiao, Y.; Li, L.H.; Xing, T.; Chen, Y.; Jaroniec, M.; Qiao, S.Z. Toward Design of Synergistically Active Carbon-Based Catalysts for Electrocatalytic Hydrogen Evolution. *ACS Nano* **2014**, *8*, 5290–5296, doi:10.1021/nn501434a.
67. Guo, D.; Shibuya, R.; Akiba, C.; Saji, S.; Kondo, T.; Nakamura, J. Active Sites of Nitrogen-Doped Carbon Materials for Oxygen Reduction Reaction Clarified Using Model Catalysts. *Science* **2016**, *351*, 361–365, doi:10.1126/science.aad0832.
68. Zhao, Z.; Li, M.; Zhang, L.; Dai, L.; Xia, Z. Design Principles for Heteroatom-Doped Carbon Nanomaterials as Highly Efficient Catalysts for Fuel Cells and Metal-Air Batteries. *Adv. Mater.* **2015**, *27*, 6834–6840, doi:10.1002/adma.201503211.
69. Pinto, H.; Markevich, A. Electronic and Electrochemical Doping of Graphene by Surface Adsorbates. *Beilstein J. Nanotechnol.* **2014**, *5*, 1842–1848, doi:10.3762/bjnano.5.195.
70. Kepaptsoglou, D.; Hardcastle, T.P.; Seabourne, C.R.; Bangert, U.; Zan, R.; Amani, J.A.; Hofsäss, H.; Nicholls, R.J.; Brydson, R.M.D.; Scott, A.J.; et al. Electronic Structure Modification of Ion Implanted Graphene: The Spectroscopic Signatures of p- and n-Type Doping. *ACS Nano* **2015**, *9*, 11398–11407, doi:10.1021/acsnano.5b05305.

71. Chauhan, S.S.; Srivastava, P.; Shrivastava, A.K. Electronic and Transport Properties of Boron and Nitrogen Doped Graphene Nanoribbons: An Ab Initio Approach. *Appl. Nanosci.* **2014**, *4*, 461–467, doi:10.1007/s13204-013-0220-2.
72. Chatterjee, K.; Ashokkumar, M.; Gullapalli, H.; Gong, Y.; Vajtai, R.; Thanikaivelan, P.; Ajayan, P.M. Nitrogen-Rich Carbon Nano-Onions for Oxygen Reduction Reaction. *Carbon* **2018**, *130*, 645–651, doi:10.1016/j.carbon.2018.01.052.
73. Sa, Y.J.; Park, C.; Jeong, H.Y.; Park, S.-H.; Lee, Z.; Kim, K.T.; Park, G.-G.; Joo, S.H. Carbon Nanotubes/Heteroatom-Doped Carbon Core-Sheath Nanostructures as Highly Active, Metal-Free Oxygen Reduction Electrocatalysts for Alkaline Fuel Cells. *Angew. Chem. Int. Ed.* **2014**, *53*, 4102–4106, doi:10.1002/anie.201307203.
74. Chen, J.; Han, Y.; Kong, X.; Deng, X.; Park, H.J.; Guo, Y.; Jin, S.; Qi, Z.; Lee, Z.; Qiao, Z.; et al. The Origin of Improved Electrical Double-Layer Capacitance by Inclusion of Topological Defects and Dopants in Graphene for Supercapacitors. *Angew. Chem. Int. Ed.* **2016**, *55*, 13822–13827, doi:10.1002/anie.201605926.
75. Sikeyi, L.L.; Ntuli, T.D.; Mongwe, T.H.; Maxakato, N.W.; Carleschi, E.; Doyle, B.P.; Coville, N.J.; Maubane-Nkadimeng, M.S. Microwave Assisted Synthesis of Nitrogen Doped and Oxygen Functionalized Carbon Nano Onions Supported Palladium Nanoparticles as Hybrid Anodic Electrocatalysts for Direct Alkaline Ethanol Fuel Cells. *Int. J. Hydrog. Energy* **2021**, *46*, 10862–10875, doi:10.1016/j.ijhydene.2020.12.154.
76. Sedelnikova, O.V.; Fedoseeva, Yu.V.; Romanenko, A.I.; Gusel'nikov, A.V.; Vilkov, O.Yu.; Maksimovskiy, E.A.; Bychanok, D.S.; Kuzhir, P.P.; Bulusheva, L.G.; Okotrub, A.V. Effect of Boron and Nitrogen Additives on Structure and Transport Properties of Arc-Produced Carbon. *Carbon* **2019**, *143*, 660–668, doi:10.1016/j.carbon.2018.11.071.
77. Umrao, S.; Gupta, T.K.; Kumar, S.; Singh, V.K.; Sultania, M.K.; Jung, J.H.; Oh, I.-K.; Srivastava, A. Microwave-Assisted Synthesis of Boron and Nitrogen Co-Doped Reduced Graphene Oxide for the Protection of Electromagnetic Radiation in Ku-Band. *ACS Appl. Mater. Interfaces* **2015**, *7*, 19831–19842, doi:10.1021/acsami.5b05890.
78. Shaikh, A.; Singh, B.K.; Mohapatra, D.; Parida, S. Nitrogen-Doped Carbon Nano-Onions as a Metal-Free Electrocatalyst. *Electrocatalysis* **2019**, *10*, 222–231, doi:10.1007/s12678-019-00514-9.
79. Jia, Y.; Zhang, L.; Du, A.; Gao, G.; Chen, J.; Yan, X.; Brown, C.L.; Yao, X. Defect Graphene as a Trifunctional Catalyst for Electrochemical Reactions. *Adv. Mater.* **2016**, *28*, 9532–9538, doi:10.1002/adma.201602912.
80. Xiao, Z.; Mou, X.; Meng, X.; Yang, Q.; Ma, Y.; Zhao, N.; Huang, X.; Shaislamov, U.; Kong, D.; Zhi, L. Electrifying Schiff-Based Networks as Model Catalysts towards Deeply Understanding the Crucial Role of Sp2-Carbon in Nitrogen-Doped Carbocatalyst for Oxygen Reduction Reaction. *Appl. Surf. Sci.* **2022**, *599*, 153961, doi:10.1016/j.apsusc.2022.153961.
81. Masemola, C.M.; Moloto, N.; Tetana, Z.N.; Gqoba, S.S.; Mubiayi, P.K.; Linganiso, E.C. N-Doped Graphene Quantum Dot-Modified Polyaniline for Room-Temperature Sensing of Alcohol Vapors. *Mater. Chem. Phys.* **2022**, *287*, 126229, doi:10.1016/j.matchemphys.2022.126229.
82. Savilov, S.V.; Arkhipova, E.A.; Ivanov, A.S.; Maslakov, K.I.; Shen, Z.; Aldoshin, S.M.; Lunin, V.V. Pyrolytic Synthesis and Characterization of N-Doped Carbon Nanoflakes for Electrochemical Applications. *Mater. Res. Bull.* **2015**, *69*, 7–12, doi:10.1016/j.materresbull.2014.12.057.
83. Kakaei, K.; Balavandi, A. Synthesis of Halogen-Doped Reduced Graphene Oxide Nanosheets as Highly Efficient Metal-Free Electrocatalyst for Oxygen Reduction Reaction. *J. Colloid Interface Sci.* **2016**, *463*, 46–54, doi:10.1016/j.jcis.2015.10.030.
84. Pham, C.V.; Britton, B.; Böhm, T.; Holdcroft, S.; Thiele, S. Doped, Defect-Enriched Carbon Nanotubes as an Efficient Oxygen Reduction Catalyst for Anion Exchange Membrane Fuel Cells. *Adv. Mater. Interfaces* **2018**, *5*, 1800184, doi:10.1002/admi.201800184.
85. Lai, Q.; Wei, K.; Tang, Z.; Liu, X.; Zheng, J.; Liang, Y. Edge Reconfiguration of N, P-Codoped Carbon Boosts Oxygen Reduction Electrocatalysis. *J. Mater. Sci.* **2021**, *56*, 19577–19588, doi:10.1007/s10853-021-06484-y.
86. Xia, C.; Hai, X.; Chen, X.-W.; Wang, J.-H. Simultaneously Fabrication of Free and Solidified N, S-Doped Graphene Quantum Dots via a Facile Solvent-Free Synthesis Route for Fluorescent Detection. *Talanta* **2017**, *168*, 269–278, doi:10.1016/j.talanta.2017.03.040.
87. Camisasca, A.; Sacco, A.; Brescia, R.; Giordani, S. Boron/Nitrogen-Codoped Carbon Nano-Onion Electrocatalysts for the Oxygen Reduction Reaction. *ACS Appl. Nano Mater.* **2018**, *1*, 5763–5773, doi:10.1021/acsanm.8b01430.
88. Domga; Karnan, M.; Oladoyinbo, F.; Noumi, G.B.; Tchatchueng, J.B.; Sieliechi, M.J.; Sathish, M.; Pattanayak, D.K. A Simple, Economical One-Pot Microwave Assisted Synthesis of Nitrogen and Sulfur Co-Doped Graphene for High Energy Supercapacitors. *Electrochimica Acta* **2020**, *341*, 135999, doi:10.1016/j.electacta.2020.135999.
89. Zhao, Y.; Yang, L.; Chen, S.; Wang, X.; Ma, Y.; Wu, Q.; Jiang, Y.; Qian, W.; Hu, Z. Can Boron and Nitrogen Co-Doping Improve Oxygen Reduction Reaction Activity of Carbon Nanotubes? *J. Am. Chem. Soc.* **2013**, *135*, 1201–1204, doi:10.1021/ja310566z.

90. Zheng, Y.; Jiao, Y.; Ge, L.; Jaroniec, M.; Qiao, S.Z. Two-Step Boron and Nitrogen Doping in Graphene for Enhanced Synergistic Catalysis. *Angew. Chem. Int. Ed.* **2013**, *52*, 3110–3116, doi:10.1002/anie.201209548.
91. Tang, C.; Zhang, Q. Nanocarbon for Oxygen Reduction Electrocatalysis: Dopants, Edges, and Defects. *Adv. Mater.* **2017**, *29*, 1604103, doi:10.1002/adma.201604103.
92. Miller, D. *Building a Project Work Breakdown Structure: Visualizing Objectives, Deliverables, Activities, and Schedules*; ESI International Project Management Series; Auerbach Publications, 2008; Vol. 20085940; ISBN 978-1-4200-6969-3.
93. Portet, C.; Yushin, G.; Gogotsi, Y. Electrochemical Performance of Carbon Onions, Nanodiamonds, Carbon Black and Multiwalled Nanotubes in Electrical Double Layer Capacitors. *Carbon* **2007**, *45*, 2511–2518, doi:10.1016/j.carbon.2007.08.024.
94. Pech, D.; Brunet, M.; Durou, H.; Huang, P.; Mochalin, V.; Gogotsi, Y.; Taberna, P.-L.; Simon, P. Ultrahigh-Power Micrometre-Sized Supercapacitors Based on Onion-like Carbon. *Nat. Nanotechnol.* **2010**, *5*, 651–654, doi:10.1038/nnano.2010.162.
95. Zeiger, M.; Jäckel, N.; Aslan, M.; Weingarth, D.; Presser, V. Understanding Structure and Porosity of Nanodiamond-Derived Carbon Onions. *Carbon* **2015**, *84*, 584–598, doi:10.1016/j.carbon.2014.12.050.
96. Bandaru, P.R.; Yamada, H.; Narayanan, R.; Hoefer, M. Charge Transfer and Storage in Nanostructures. *Mater. Sci. Eng. R Rep.* **2015**, *96*, 1–69, doi:10.1016/j.mser.2015.06.001.
97. Bagge-Hansen, M.; Bastea, S.; Hammons, J.A.; Nielsen, M.H.; Lauderbach, L.M.; Hodgin, R.L.; Pagoria, P.; May, C.; Aloni, S.; Jones, A.; et al. Detonation Synthesis of Carbon Nano-Onions via Liquid Carbon Condensation. *Nat. Commun.* **2019**, *10*, doi:10.1038/s41467-019-11666-z.
98. Moussa, G.; Matei Ghimbeu, C.; Taberna, P.-L.; Simon, P.; Vix-Guterl, C. Relationship between the Carbon Nano-Onions (CNOs) Surface Chemistry/Defects and Their Capacitance in Aqueous and Organic Electrolytes. *Carbon* **2016**, *105*, 628–637, doi:10.1016/j.carbon.2016.05.010.
99. Borgohain, R.; Li, J.; Selegue, J.P.; Cheng, Y.-T. Electrochemical Study of Functionalized Carbon Nano-Onions for High-Performance Supercapacitor Electrodes. *J. Phys. Chem. C* **2012**, *116*, 15068–15075, doi:10.1021/jp301642s.
100. Kumar, R.; Sahoo, S.; Joanni, E.; Singh, R.K.; Kar, K.K. Microwave as a Tool for Synthesis of Carbon-Based Electrodes for Energy Storage. *ACS Appl. Mater. Interfaces* **2022**, *14*, 20306–20325, doi:10.1021/acsami.1c15934.
101. Schwenke, A.M.; Hoeppener, S.; Schubert, U.S. Synthesis and Modification of Carbon Nanomaterials Utilizing Microwave Heating. *Adv. Mater.* **2015**, *27*, 4113–4141, doi:10.1002/adma.201500472.
102. Kim, T.; Lee, J.; Lee, K.-H. Microwave Heating of Carbon-Based Solid Materials. *Carbon Lett.* **2014**, *15*, 15–24, doi:10.5714/CL.2014.15.1.015.
103. Menéndez, J.A.; Arenillas, A.; Fidalgo, B.; Fernández, Y.; Zubizarreta, L.; Calvo, E.G.; Bermúdez, J.M. Microwave Heating Processes Involving Carbon Materials. *Fuel Process. Technol.* **2010**, *91*, 1–8, doi:10.1016/j.fuproc.2009.08.021.
104. Liu, Z.; Zhang, L.; Poyraz, S.; Smith, J.; Kushvaha, V.; Tippur, H.; Zhang, X. An Ultrafast Microwave Approach towards Multi-Component and Multi-Dimensional Nanomaterials. *RSC Adv.* **2014**, *4*, 9308, doi:10.1039/c3ra47086e.
105. Slocombe, D.; Porch, A.; Bustarret, E.; Williams, O.A. Microwave Properties of Nanodiamond Particles. *Appl. Phys. Lett.* **2013**, *102*, 244102, doi:10.1063/1.4809823.
106. Chen, X.; Tian, X.; Zhou, Z.; Jiang, M.; Lu, J.; Wang, Y.; Wang, L. Effective Improvement in Microwave Absorption by Uniform Dispersion of Nanodiamond in Polyaniline through *in-Situ* Polymerization. *Appl. Phys. Lett.* **2015**, *106*, 233103, doi:10.1063/1.4922315.
107. Yoon, B.-J.; Hong, E.H.; Jee, S.E.; Yoon, D.-M.; Shim, D.-S.; Son, G.-Y.; Lee, Y.J.; Lee, K.-H.; Kim, H.S.; Park, C.G. Fabrication of Flexible Carbon Nanotube Field Emitter Arrays by Direct Microwave Irradiation on Organic Polymer Substrate. *J. Am. Chem. Soc.* **2005**, *127*, 8234–8235, doi:10.1021/ja043823n.
108. Ma, Z.; Yu, J.; Dai, S. Preparation of Inorganic Materials Using Ionic Liquids. *Adv. Mater.* **2010**, *22*, 261–285, doi:10.1002/adma.200900603.
109. Zhao, H.; Sun, C.; Jin, Z.; Wang, D.-W.; Yan, X.; Chen, Z.; Zhu, G.; Yao, X. Carbon for the Oxygen Reduction Reaction: A Defect Mechanism. *J. Mater. Chem. A* **2015**, *3*, 11736–11739, doi:10.1039/C5TA02229K.
110. Pentsak, E.O.; Gordeev, E.G.; Ananikov, V.P. Noninnocent Nature of Carbon Support in Metal/Carbon Catalysts: Etching/Pitting vs Nanotube Growth under Microwave Irradiation. *ACS Catal.* **2014**, *4*, 3806–3814, doi:10.1021/cs500934g.
111. Bajpai, R.; Wagner, H.D. Fast Growth of Carbon Nanotubes Using a Microwave Oven. *Carbon* **2015**, *82*, 327–336, doi:10.1016/j.carbon.2014.10.077.
112. Hsin, Y.-L.; Lin, C.-F.; Liang, Y.-C.; Hwang, K.C.; Horng, J.-C.; Ho, J.A.; Lin, C.-C.; Hwu, J.R. Microwave Arcing Induced Formation and Growth Mechanisms of Core/Shell Metal/Carbon Nanoparticles in Organic Solutions: Formation and Growth Mechanisms of Core/Shell Nanoparticles. *Adv. Funct. Mater.* **2008**, *18*, 2048–2056, doi:10.1002/adfm.200701407.

113. Liu, Z.; Wang, J.; Kushvaha, V.; Poyraz, S.; Tippur, H.; Park, S.; Kim, M.; Liu, Y.; Bar, J.; Chen, H.; et al. Poptube Approach for Ultrafast Carbon Nanotube Growth. *Chem. Commun.* **2011**, *47*, 9912, doi:10.1039/c1cc13359d.
114. Takagi, Y.; Tauchi, L.; Nguyen-Tran, H.-D.; Ohta, T.; Shimizu, M.; Ohta, K. Development of a Novel Method to Synthesize Carbon Nanotubes from Granulated Polystyrene and Nickel Nanoparticles by Microwave Heating. *J. Mater. Chem.* **2011**, *21*, 14569, doi:10.1039/c1jm12069g.
115. Li, S.; Guo, C.; Qiao, yuqing Microwave-Assisted Synthesis of Functionalized Graphene Hydrogels for High Performance Supercapacitors. *Mater. Sci. Eng. B* **2021**, *273*, 115407, doi:10.1016/j.mseb.2021.115407.
116. Rosli, N.H.A.; Lau, K.S.; Winie, T.; Chin, S.X.; Chia, C.H. Synergistic Effect of Sulfur-Doped Reduced Graphene Oxide Created via Microwave-Assisted Synthesis for Supercapacitor Applications. *Diam. Relat. Mater.* **2021**, *120*, 108696, doi:10.1016/j.diamond.2021.108696.
117. Ma, J.; Yamamoto, Y.; Su, C.; Badhulika, S.; Fukuhara, C.; Kong, C.Y. One-Pot Microwave-Assisted Synthesis of Porous Reduced Graphene Oxide as an Electrode Material for High Capacitance Supercapacitor. *Electrochimica Acta* **2021**, *386*, 138439, doi:10.1016/j.electacta.2021.138439.
118. Kim, T.; Chang Kang, H.; Thanh Tung, T.; Don Lee, J.; Kim, H.; Seok Yang, W.; Gyu Yoon, H.; Suh, K.S. Ionic Liquid-Assisted Microwave Reduction of Graphite Oxide for Supercapacitors. *RSC Adv.* **2012**, *2*, 8808, doi:10.1039/c2ra21400h.
119. Qureshi, S.S.; Shah, V.; Nizamuddin, S.; Mubarak, N.M.; Karri, R.R.; Dehghani, M.H.; Ramesh, S.; Khalid, M.; Rahman, M.E. Microwave-Assisted Synthesis of Carbon Nanotubes for the Removal of Toxic Cationic Dyes from Textile Wastewater. *J. Mol. Liq.* **2022**, *356*, 119045, doi:10.1016/j.molliq.2022.119045.
120. Ali, M.; Riaz, R.; Anjum, A.S.; Sun, K.C.; Li, H.; Ahn, S.; Jeong, S.H.; Ko, M.J. Microwave-Assisted Ultrafast in-Situ Growth of N-Doped Carbon Quantum Dots on Multiwalled Carbon Nanotubes as an Efficient Electrocatalyst for Photovoltaics. *J. Colloid Interface Sci.* **2021**, *586*, 349–361, doi:10.1016/j.jcis.2020.10.098.
121. Li, J.; Tang, Y.; Jin, R.; Meng, Q.; Chen, Y.; Long, X.; Wang, L.; Guo, H.; Zhang, S. Ultrasonic-Microwave Assisted Synthesis of GO/g-C3N4 Composites for Efficient Photocatalytic H2 Evolution. *Solid State Sci.* **2019**, *97*, 105990, doi:10.1016/j.solidstatesciences.2019.105990.
122. Wang, W.; Jin, J.; Wu, Y.; Zhang, W.; Jiang, H.; Li, X.; Wang, G. Unique Holey Graphene/Carbon Dots Frameworks by Microwave-Initiated Chain Reduction for High-Performance Compressible Supercapacitors and Reusable Oil/Water Separation. *J. Mater. Chem. A* **2019**, *7*, 22054–22062, doi:10.1039/C9TA06083A.
123. Jessl, S.; Copic, D.; Engelke, S.; Ahmad, S.; De Volder, M. Hydrothermal Coating of Patterned Carbon Nanotube Forest for Structured Lithium-Ion Battery Electrodes. *Small* **2019**, *15*, 1901201, doi:10.1002/smll.201901201.
124. Kumar, R.; Singh, R.K.; Tiwari, V.S.; Yadav, A.; Savu, R.; Vaz, A.R.; Moshkalev, S.A. Enhanced Magnetic Performance of Iron Oxide Nanoparticles Anchored Pristine/ N-Doped Multi-Walled Carbon Nanotubes by Microwave-Assisted Approach. *J. Alloys Compd.* **2017**, *695*, 1793–1801, doi:10.1016/j.jallcom.2016.11.010.
125. Sun, Y.; Du, X.; Zhang, J.; Huang, N.; Yang, L.; Sun, X. Microwave-Assisted Preparation and Improvement Mechanism of Carbon Nanotube@NiMn2O4 Core-Shell Nanocomposite for High Performance Asymmetric Supercapacitors. *J. Power Sources* **2020**, *473*, 228609, doi:10.1016/j.jpowsour.2020.228609.
126. Xu, Z.; Li, Z.; Tan, X.; Holt, C.M.B.; Zhang, L.; Amirkhiz, B.S.; Mitlin, D. Supercapacitive Carbon Nanotube-Cobalt Molybdate Nanocomposites Prepared via Solvent-Free Microwave Synthesis. *RSC Adv.* **2012**, *2*, 2753, doi:10.1039/c2ra01300b.
127. Zheng, Y.; Tian, Y.; Liu, S.; Tan, X.; Wang, S.; Guo, Q.; Luo, J.; Li, Z. One-Step Microwave Synthesis of NiO/NiS@CNT Nanocomposites for High-Cycling-Stability Supercapacitors. *J. Alloys Compd.* **2019**, *806*, 170–179, doi:10.1016/j.jallcom.2019.07.213.
128. Chakraborty, S.; Simon, R.; Vadakkekara, A.; N.L., M. Microwave Assisted Synthesis of Poly(Ortho-Phenylenediamine-Co-Aniline) and Functionalised Carbon Nanotube Nanocomposites for Fabric-Based Supercapacitors. *Electrochimica Acta* **2022**, *403*, 139678, doi:10.1016/j.electacta.2021.139678.
129. Wang, Y.; Zhang, W.; Guo, X.; Liu, Y.; Zheng, Y.; Zhang, M.; Li, R.; Peng, Z.; Zhang, Y.; Zhang, T. One-Step Microwave-Hydrothermal Preparation of NiS/RGO Hybrid for High-Performance Symmetric Solid-State Supercapacitor. *Appl. Surf. Sci.* **2020**, *514*, 146080, doi:10.1016/j.apsusc.2020.146080.
130. Kumar, R.; Singh, R.K.; Alaferdov, A.V.; Moshkalev, S.A. Rapid and Controllable Synthesis of Fe3O4 Octahedral Nanocrystals Embedded-Reduced Graphene Oxide Using Microwave Irradiation for High Performance Lithium-Ion Batteries. *Electrochimica Acta* **2018**, *281*, 78–87, doi:10.1016/j.electacta.2018.05.157.
131. Bae, S.-H.; Karthikeyan, K.; Lee, Y.-S.; Oh, I.-K. Microwave Self-Assembly of 3D Graphene-Carbon Nanotube-Nickel Nanostructure for High Capacity Anode Material in Lithium Ion Battery. *Carbon* **2013**, *64*, 527–536, doi:10.1016/j.carbon.2013.08.003.
132. Kumar, R.; Singh, R.K.; Savu, R.; Dubey, P.K.; Kumar, P.; Moshkalev, S.A. Microwave-Assisted Synthesis of Void-Induced Graphene-Wrapped Nickel Oxide Hybrids for Supercapacitor Applications. *RSC Adv.* **2016**, *6*, 26612–26620, doi:10.1039/C6RA00426A.

133. Kumar, R.; Youssry, S.M.; Soe, H.M.; Abdel-Galeil, M.M.; Kawamura, G.; Matsuda, A. Honeycomb-like Open-Edged Reduced-Graphene-Oxide-Enclosed Transition Metal Oxides (NiO/Co3O4) as Improved Electrode Materials for High-Performance Supercapacitor. *J. Energy Storage* **2020**, *30*, 101539, doi:10.1016/j.est.2020.101539.
134. Fang, J.; Li, M.; Li, Q.; Zhang, W.; Shou, Q.; Liu, F.; Zhang, X.; Cheng, J. Microwave-Assisted Synthesis of CoAl-Layered Double Hydroxide/Graphene Oxide Composite and Its Application in Supercapacitors. *Electrochimica Acta* **2012**, *85*, 248–255, doi:10.1016/j.electacta.2012.08.078.
135. Li, M.; Cheng, J.P.; Fang, J.H.; Yang, Y.; Liu, F.; Zhang, X.B. NiAl-Layered Double Hydroxide/Reduced Graphene Oxide Composite: Microwave-Assisted Synthesis and Supercapacitive Properties. *Electrochimica Acta* **2014**, *134*, 309–318, doi:10.1016/j.electacta.2014.04.141.
136. Liu, T.; Chai, H.; Jia, D.; Su, Y.; Wang, T.; Zhou, W. Rapid Microwave-Assisted Synthesis of Mesoporous NiMoO4 Nanorod/Reduced Graphene Oxide Composites for High-Performance Supercapacitors. *Electrochimica Acta* **2015**, *180*, 998–1006, doi:10.1016/j.electacta.2015.07.175.
137. Reddy, B.J.; Vickraman, P.; Justin, A.S. Asymmetric Supercapacitor Device Performance Based on Microwave Synthesis of N-Doped Graphene/Nickel Sulfide Nanocomposite. *J. Mater. Sci.* **2019**, *54*, 6361–6373, doi:10.1007/s10853-018-03314-6.
138. Kumar, R.; Abdel-Galeil, M.M.; Ya, K.Z.; Fujita, K.; Tan, W.K.; Matsuda, A. Facile and Fast Microwave-Assisted Formation of Reduced Graphene Oxide-Wrapped Manganese Cobaltite Ternary Hybrids as Improved Supercapacitor Electrode Material. *Appl. Surf. Sci.* **2019**, *481*, 296–306, doi:10.1016/j.apsusc.2019.03.085.
139. Nagaraju, P.; Arivanandhan, M.; Alsalme, A.; Alghamdi, A.; Jayavel, R. Enhanced Electrochemical Performance of α-MoO $_3$ /Graphene Nanocomposites Prepared by an *in Situ* Microwave Irradiation Technique for Energy Storage Applications. *RSC Adv.* **2020**, *10*, 22836–22847, doi:10.1039/C9RA10873D.
140. Miao, C.; Yin, X.; Xia, G.; Zhu, K.; Ye, K.; Wang, Q.; Yan, J.; Cao, D.; Wang, G. Facile Microwave-Assisted Synthesis of Cobalt Diselenide/Reduced Graphene Oxide Composite for High-Performance Supercapacitors. *Appl. Surf. Sci.* **2021**, *543*, 148811, doi:10.1016/j.apsusc.2020.148811.
141. Masikhwa, T.M.; Madito, M.J.; Bello, A.; Lekitima, J.; Manyala, N. Microwave-Assisted Synthesis of Cobalt Sulphide Nanoparticle Clusters on Activated Graphene Foam for Electrochemical Supercapacitors. *RSC Adv.* **2017**, *7*, 20231–20240, doi:10.1039/C7RA02204B.
142. Sridhar, V.; Park, H. Manganese Nitride Stabilized on Reduced Graphene Oxide Substrate for High Performance Sodium Ion Batteries, Super-Capacitors and EMI Shielding. *J. Alloys Compd.* **2019**, *808*, 151748, doi:10.1016/j.jallcom.2019.151748.
143. Vimuna, V.M.; Athira, A.R.; Dinesh Babu, K.V.; Xavier, T.S. Simultaneous Stirring and Microwave Assisted Synthesis of Nanoflakes MnO2/RGO Composite Electrode Material for Symmetric Supercapacitor with Enhanced Electrochemical Performance. *Diam. Relat. Mater.* **2020**, *110*, 108129, doi:10.1016/j.diamond.2020.108129.
144. Kumar, R.; da Silva, E.T.S.G.; Singh, R.K.; Savu, R.; Alaferdov, A.V.; Fonseca, L.C.; Carossi, L.C.; Singh, A.; Khandka, S.; Kar, K.K.; et al. Microwave-Assisted Synthesis of Palladium Nanoparticles Intercalated Nitrogen Doped Reduced Graphene Oxide and Their Electrocatalytic Activity for Direct-Ethanol Fuel Cells. *J. Colloid Interface Sci.* **2018**, *515*, 160–171, doi:10.1016/j.jcis.2018.01.028.
145. Kumar, R.; Savu, R.; Singh, R.K.; Joanni, E.; Singh, D.P.; Tiwari, V.S.; Vaz, A.R.; da Silva, E.T.S.G.; Maluta, J.R.; Kubota, L.T.; et al. Controlled Density of Defects Assisted Perforated Structure in Reduced Graphene Oxide Nanosheets-Palladium Hybrids for Enhanced Ethanol Electro-Oxidation. *Carbon* **2017**, *117*, 137–146, doi:10.1016/j.carbon.2017.02.065.
146. Ma, T.; Liu, H.; Wang, Y.; Zhang, M. Rapid Construction of Three-Dimensional Sulfur Doped Graphene Supported by NiFeS2 Interconnected Networks as Convenient Electron/Ion Transport Channels for Flexible Supercapacitors. *Electrochimica Acta* **2019**, *309*, 1–10, doi:10.1016/j.electacta.2019.04.079.
147. Kumar, R.; Oh, J.-H.; Kim, H.-J.; Jung, J.-H.; Jung, C.-H.; Hong, W.G.; Kim, H.-J.; Park, J.-Y.; Oh, I.-K. Nanohole-Structured and Palladium-Embedded 3D Porous Graphene for Ultrahigh Hydrogen Storage and CO Oxidation Multifunctionalities. *ACS Nano* **2015**, *9*, 7343–7351, doi:10.1021/acsnano.5b02337.
148. Khamlich, S.; Mokrani, T.; Dhlamini, M.S.; Mothudi, B.M.; Maaza, M. Microwave-Assisted Synthesis of Simonkolleite Nanoplatelets on Nickel Foam–Graphene with Enhanced Surface Area for High-Performance Supercapacitors. *J. Colloid Interface Sci.* **2016**, *461*, 154–161, doi:10.1016/j.jcis.2015.09.033.
149. Zhao, F.; Xie, D.; Huang, W.; Song, X.; Aurang Zeb Gul Sial, M.; Wu, H.; Deng, F.; Zhang, Q.; Zou, J.; Zeng, X. Defect-Rich Honeycomb-like Nickel Cobalt Sulfides on Graphene through Rapid Microwave-Induced Synthesis for Ultrahigh Rate Supercapacitors. *J. Colloid Interface Sci.* **2020**, *580*, 160–170, doi:10.1016/j.jcis.2020.06.091.
150. Sridhar, V.; Kim, H.-J.; Jung, J.-H.; Lee, C.; Park, S.; Oh, I.-K. Defect-Engineered Three-Dimensional Graphene–Nanotube–Palladium Nanostructures with Ultrahigh Capacitance. *ACS Nano* **2012**, *6*, 10562–10570, doi:10.1021/nn3046133.

151. Yan, K.; Sun, X.; Ying, S.; Cheng, W.; Deng, Y.; Ma, Z.; Zhao, Y.; Wang, X.; Pan, L.; Shi, Y. Ultrafast Microwave Synthesis of Rambutan-like CMK-3/Carbon Nanotubes Nanocomposites for High-Performance Supercapacitor Electrode Materials. *Sci. Rep.* **2020**, *10*, 6227, doi:10.1038/s41598-020-63204-3.
152. Borges-Vilches, J.; Figueroa, T.; Guajardo, S.; Meléndrez, M.; Fernández, K. Development of Gelatin Aerogels Reinforced with Graphene Oxide by Microwave-Assisted Synthesis: Influence of the Synthesis Conditions on Their Physicochemical Properties. *Polymer* **2020**, *208*, 122951, doi:10.1016/j.polymer.2020.122951.
153. Cuenca, J.A.; Thomas, E.; Mandal, S.; Williams, O.; Porch, A. Microwave Determination of Sp2 Carbon Fraction in Nanodiamond Powders. *Carbon* **2015**, *81*, 174–178, doi:10.1016/j.carbon.2014.09.046.
154. Adam, M.; Hart, A.; Stevens, L.A.; Wood, J.; Robinson, J.P.; Rigby, S.P. Microwave Synthesis of Carbon Onions in Fractal Aggregates Using Heavy Oil as a Precursor. *Carbon* **2018**, *138*, 427–435, doi:10.1016/j.carbon.2018.07.066.
155. Ahmed, G.H.G.; Laíño, R.B.; Calzón, J.A.G.; García, M.E.D. Facile Synthesis of Water-Soluble Carbon Nano-Onions under Alkaline Conditions. *Beilstein J. Nanotechnol.* **2016**, *7*, 758–766, doi:10.3762/bjnano.7.67.
156. Vadahanambi, S.; Jung, J.-H.; Kumar, R.; Kim, H.-J.; Oh, I.-K. An Ionic Liquid-Assisted Method for Splitting Carbon Nanotubes to Produce Graphene Nano-Ribbons by Microwave Radiation. *Carbon* **2013**, *53*, 391–398, doi:10.1016/j.carbon.2012.11.029.
157. Kumar, R.; Youssry, S.M.; Joanni, E.; Sahoo, S.; Kawamura, G.; Matsuda, A. Microwave-Assisted Synthesis of Iron Oxide Homogeneously Dispersed on Reduced Graphene Oxide for High-Performance Supercapacitor Electrodes. *J. Energy Storage* **2022**, *56*, 105896, doi:10.1016/j.est.2022.105896.
158. Yang, S.; Li, S.; Song, L.; Lv, Y.; Duan, Z.; Li, C.; Praeg, R.F.; Gao, D.; Chen, G. Defect-Density Control of Platinum-Based Nanoframes with High-Index Facets for Enhanced Electrochemical Properties. *Nano Res.* **2019**, *12*, 2881–2888, doi:10.1007/s12274-019-2530-5.
159. Lu, J.; Luo, L.; Yin, S.; Hasan, S.W.; Tsiakaras, P. Oxygen Reduction Reaction over PtFeM (M = Mo, V, W) Alloy Electrocatalysts: Role of the Compressive Strain Effect on Pt. *ACS Sustain. Chem. Eng.* **2019**, *7*, 16209–16214, doi:10.1021/acssuschemeng.9b03176.
160. Luo, M.; Zhao, Z.; Zhang, Y.; Sun, Y.; Xing, Y.; Lv, F.; Yang, Y.; Zhang, X.; Hwang, S.; Qin, Y.; et al. PdMo Bimetallene for Oxygen Reduction Catalysis. *Nature* **2019**, *574*, 81–85, doi:10.1038/s41586-019-1603-7.
161. Back, S.; Kim, J.-H.; Kim, Y.-T.; Jung, Y. Bifunctional Interface of Au and Cu for Improved CO_2 Electroreduction. *ACS Appl. Mater. Interfaces* **2016**, *8*, 23022–23027, doi:10.1021/acsami.6b05903.
162. Rondinini, S.; Aricci, G.; Krpetić, Ž.; Locatelli, C.; Minguzzi, A.; Porta, F.; Vertova, A. Electroreductions on Silver-Based Electrocatalysts: The Use of Ag Nanoparticles for $CHCl_3$ to CH_4 Conversion. *Fuel Cells* **2009**, *9*, 253–263, doi:10.1002/fuce.200800083.
163. Wang, Y.; Zhang, L.; Yin, K.; Zhang, J.; Gao, H.; Liu, N.; Peng, Z.; Zhang, Z. Nanoporous Iridium-Based Alloy Nanowires as Highly Efficient Electrocatalysts Toward Acidic Oxygen Evolution Reaction. *ACS Appl. Mater. Interfaces* **2019**, *11*, 39728–39736, doi:10.1021/acsami.9b09412.
164. Zhu, J.; Chen, Z.; Xie, M.; Lyu, Z.; Chi, M.; Mavrikakis, M.; Jin, W.; Xia, Y. Iridium-Based Cubic Nanocages with 1.1-Nm-Thick Walls: A Highly Efficient and Durable Electrocatalyst for Water Oxidation in an Acidic Medium. *Angew. Chem. Int. Ed.* **2019**, *58*, 7244–7248, doi:10.1002/anie.201901732.
165. Liu, X.; Dai, L. Carbon-Based Metal-Free Catalysts. *Nat. Rev. Mater.* **2016**, *1*, doi:10.1038/natrevmats.2016.64.